Inorganic Chemistry

Article

pubs.acs.org/IC

Significant Influence of Coligands Toward Varying Coordination Modes of 2,2′-Bipyridine-3,3′-diol in Ruthenium Complexes

Prabir Ghosh,[†] Prasenjit Mondal,[†] Ritwika Ray,[†] Ankita Das,[†] Sukdev Bag,[†] Shaikh M. Mobin,[‡] and Goutam Kumar Lahiri*[,†]

[†]Department of Chemistry, Indian Institute of Technology Bombay, Powai, Mumbai 400076, India

[‡]Discipline of Chemistry, School of Basic Sciences, Indian Institute of Technology Indore, Indore 452017, India

Supporting Information

ABSTRACT: The varying coordination modes of the ambidentate ligand 2,2′-bipyridine-3,3′-diol (H_2L) in a set of ruthenium complexes were demonstrated with special reference to the electronic features of the coligands, including σ-donating acac$^-$ (= acetylacetonate) in $Ru^{III}(acac)_2(HL^-)$ (**1**), strongly π-accepting pap (= 2-phenylazopyridine) in $Ru^{II}(pap)_2(L^{2-})$ (**2**)/$[(pap)_2Ru^{II}(\mu\text{-}L^{2-})Ru^{II}(pap)_2](ClO_4)_2$ ([**4**]$(ClO_4)_2$), and reported moderately π-accepting bpy (= 2,2′-bypiridine) in $[Ru^{II}(bpy)_2(HL^-)]PF_6$ ([**5**]PF_6)/$[(bpy)_2Ru(\mu\text{-}L^{2-})Ru(bpy)_2](PF_6)_2$ ([**7**]$(PF_6)_2$). The single-crystal X-ray structures reveal that, in paramagnetic and electron paramagnetic resonance active **1** and reported diamagnetic [**5**]PF_6, nearly planar monoanionic HL$^-$ coordinates to the metal ion via the *N,N* donors forming a five-membered chelate ring with hydrogen-bonded O−H···O function at the backbone of the ligand framework, as has also been reported in other metal complexes. However, structurally characterized diamagnetic **2** represents O$^-$,O$^-$ bonded seven-membered chelate of fully deprotonated but twisted L^{2-}. The nonplanarity of the coordinated L^{2-} in **2** does not permit the second metal fragment $\{Ru(pap)_2\}$ or $\{Ru(bpy)_2\}$ or $\{Ru(acac)_2\}$ to bind with the available N,N donors at the back face of L^{2-}. Further, the deprotonated form of the model ligand 2,2′-biphenol (H_2L') yields $Ru^{II}(pap)_2(L'^{2-})$ (**3**); its crystal structure establishes the expected O$^-$,O$^-$ bonded seven-membered chelate of nonplanar L'^{2-} as in reported $Ru^{II}(bpy)_2(L'^{2-})$ (**6**), although $\{Ru(acac)_2\}$ metal precursor altogether fails to react with H_2L'. All attempts to make diruthenium complex from $\{Ru(acac)_2\}$ and H_2L failed; however, the corresponding $\{Ru(pap)_2^{2+}\}$ derived dimeric [**4**]$(ClO_4)_2$ was structurally characterized. It establishes the symmetric N,O$^-$/N,O$^-$ bridging mode of nonplanar L^{2-} as in reported [**7**]$(PF_6)_2$. Besides structural and spectroscopic characterization of the newly developed complexes, the ligand (HL$^-$, L^{2-}, L'^{2-}, pap)-, metal-, or mixed metal−ligand-based accessible redox processes in $\mathbf{1}^n$ (n = +2, +1, 0, −1), $\mathbf{2}^n/\mathbf{3}^n$ (n = +2, +1, 0, −1, −2), and $\mathbf{4}^n$ (n = +4, +3, +2, +1, 0, −1) were analyzed in conjunction with density functional theory calculations.

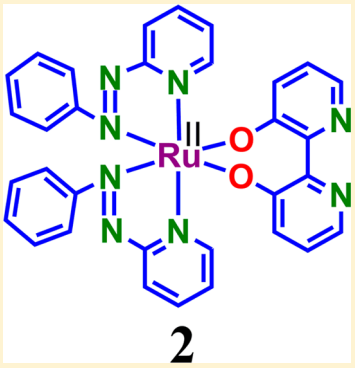

INTRODUCTION

The ambidentate ligand 2,2′-bipyridine-3,3′-diol (H_2L) encircling two dissociable protons has the potential to bind to the metal ion as a bidentate ligand but in different fashions, primarily because of suitably positioned multiple donor sets (N,N, OH,OH, and N,OH) as well as inherent rotational flexibility of the two rings about the connecting C−C single bond. At the mononuclear level, in principle H_2L can function as a neutral N,N chelator with pendant hydroxyl groups (**a**), monoanionic N,N chelator with a hydrogen-bonded O−H···O group at the backbone (**b**), dianionic O$^-$,O$^-$ chelator with free N,N donors at the backbone (**c**), and mixed donors monoanionic N,O$^-$ chelator with hydrogen-bonded O−H···N group at the backbone (**d**) (Scheme 1). Dinucleating mode includes asymmetric N,N and O$^-$,O$^-$ donor sets (**e**) and symmetric N, O$^-$ and N, O$^-$ donor sets (**f**) (Scheme 1).

In reported mononuclear complexes of Ru(II),[1,2] Cu(II),[3a−c] Co(III),[3c,d] Ir(III),[4] Pd(II),[5] Zn(II),[6] and Cd(II),[7] the H_2L ligand selectively binds to the metal ions as a monoanionic bidentate N,N chelator with the hydrogen-bonded pendant hydroxyl groups ((**b**) in Scheme 1). The binding mode (**a**) of H_2L in Scheme 1 has also been reported in $[Re^I(CO)_3Cl(H_2L)]$[8] and $[(\eta^6\text{-ind})Ru^{II}(H_2L)Cl][PF_6]$.[2] However, to the best of our knowledge the other two conceivable binding modes of H_2L at the mononuclear level, that is, dianionic O$^-$,O$^-$ (**c**) and monoanionic N,O$^-$ (**d**) in Scheme 1, have not been demonstrated so far.

On the other hand, the potential of H_2L to bridge the metal fragments has been reported in $[(bpy)_2Ru^{II}(\mu\text{-}L^{2-})Ru^{II}(bpy)_2](PF_6)_2$ (bpy = 2,2′-bipyridine), where dianionic L^{2-} bridges the metal ions through symmetric N,O$^-$/N,O$^-$ donors, ((**f**) in Scheme 1).[1a] The asymmetric bridging mode of H_2L ((**e**) in Scheme 1) is rather elusive.

The present study aims to evaluate the effect of electronic characteristics of the coligands associated with the metal ion, namely, $\{Ru(acac)_2\}$ (acac$^-$ = σ-donating acetylacetonate), $\{Ru(bpy)_2\}$ (bpy = moderately strong π-accepting 2,2′-bipyridine), and $\{Ru(pap)_2\}$ (pap = strongly π-accepting phenylazopyridine) toward the coordination mode of the

Received: February 27, 2014
Published: May 22, 2014

   dx.doi.org/10.1021/ic5004676 | *Inorg. Chem.* 2014, 53, 6094−6106

Scheme 1. Varying Binding Modes of H_2L

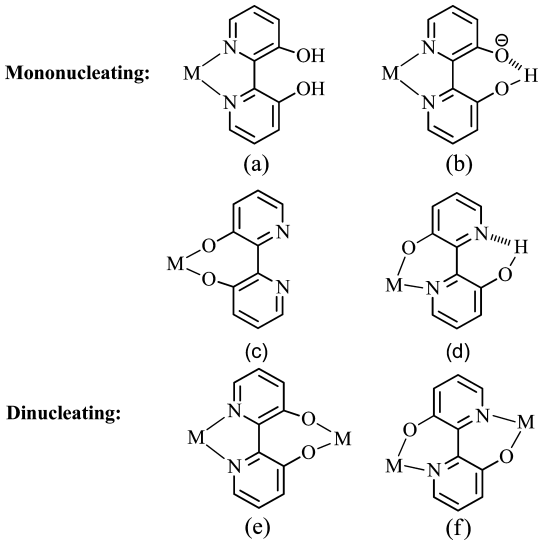

ambidentate H_2L. The article thus demonstrates coligand-dependent varying binding modes of H_2L (Scheme 1) in analogous ruthenium complexes $Ru^{III}(acac)_2(HL^-)$ (**1**), $Ru^{II}(pap)_2(L^{2-})$ (**2**), $[(pap)_2Ru^{II}(\mu\text{-}L^{2-})Ru^{II}(pap)_2](ClO_4)_2$ [**4**]$(ClO_4)_2$, $[Ru^{II}(bpy)_2(HL^-)]PF_6$ ([**5**]PF_6),[1a] and $[(bpy)_2Ru^{II}(\mu\text{-}L^{2-})Ru^{II}(bpy)_2](PF_6)_2$ [**7**]$(PF_6)_2$[1a] in combination with model complexes $Ru^{II}(pap)_2(L'^{2-})$ (**3**) and $Ru^{II}(bpy)_2(L'^{2-})$ (**6**) (H_2L': 2,2′-biphenol).[1b]

Further, electrochemical and spectral aspects of the complexes were addressed in conjunction with density functional theory (DFT) and time-dependent (TD) DFT calculations.

Note that ruthenium-arene complexes encompassing H_2L or monoanionic HL^- are reported to exhibit significant cytotoxicity toward A2780 human ovarian and 549 human lung cancer cells.[2] Moreover, metal complexes incorporating ligand frameworks with free OH or nitrogen group participate in pH-driven proton-shuttling processes,[9] which can have potential application in catalysis.[4,10]

RESULTS AND DISCUSSION

Synthesis. *Mononuclear Complexes 1–3.* The mononuclear paramagnetic $Ru^{III}(acac)_2(HL^-)$ (**1**) and diamagnetic $Ru^{II}(pap)_2(L^{2-})$ (**2**) complexes incorporating partially and fully deprotonated H_2L, respectively, (H_2L = 2,2′-bipyridine-3,3′-diol, $acac^-$ = σ-donating acetylacetonate, pap = π-accepting 2-phenylazopyridine) were obtained from the respective metal precursors $Ru^{II}(acac)_2(CH_3CN)_2$, *ctc*-$[Ru^{II}(pap)_2(EtOH)_2]^{2+}$ (*ctc* = *cis-trans-cis* with respect to solvent, pyridine, and azo nitrogens of pap, respectively[11]), and H_2L in the presence of NEt_3 as a base in refluxing ethanol (Scheme 2). The complexes were further purified by column chromatography.

The presence of three anionic ligand moieties (two $acac^-$ and HL^-) facilitates the stabilization of the Ru(III) state in **1** under aerobic reaction conditions, as has been reported in other {Ru(acac)$_2$} derived complexes.[12] However, the effect of strongly π-accepting pap was reflected in the eventual stabilization of the Ru(II) state in **2** even in combination with dianionic L^{2-}. Similar effect of π-acceptor feature of pap in stabilizing ruthenium(II) state in combination with dianionic catecholate ligand was also reported earlier.[13] The significant impact of electronic nature of the coligands "acac" versus "pap" on the metal oxidation states Ru(III) in **1** and Ru(II) in **2** was also corroborated by their Ru(II)/Ru(III) redox potentials (see later).

Crystal-structure analysis authenticates different binding modes of the H_2L ligand in **1** and **2** (see below). In **1**, the monoanionic HL^- binds to the metal ion through the usual N,N donors with hydrogen-bonded pendant hydroxyl groups, O−H···O ((**b**) in Scheme 1), as demonstrated in analogous $[Ru^{II}(bpy)_2(HL^-)]^+$ ($\mathbf{5}^+$)[1a] and other reported complexes.[2−7] However, O^-,O^- bonded L^{2-} leading to a less common seven-membered chelate ring[14] ((**c**) in Scheme 1) has been unveiled in $Ru^{II}(pap)_2(L^{2-})$ (**2**). The significant decrease in electron density on the metal ion in **2** due to the strong $(d\pi)Ru^{II} \rightarrow \pi^*(N{=}N)(pap)$ back-bonding effect[15] has indeed facilitated

Scheme 2. Representation of Complexes

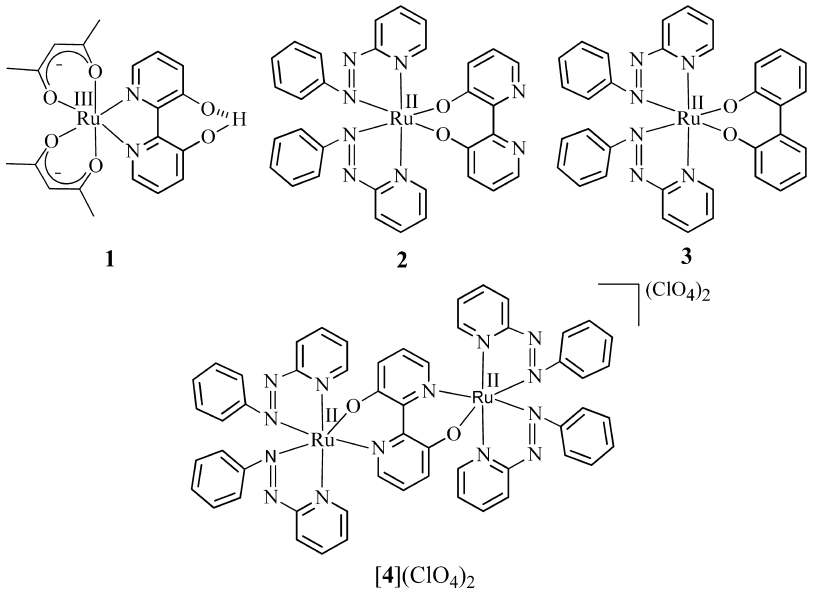

dx.doi.org/10.1021/ic5004676 | Inorg. Chem. 2014, 53, 6094−6106

Scheme 3. Reactivity Pattern of H_2L with Different Ruthenium Precursors

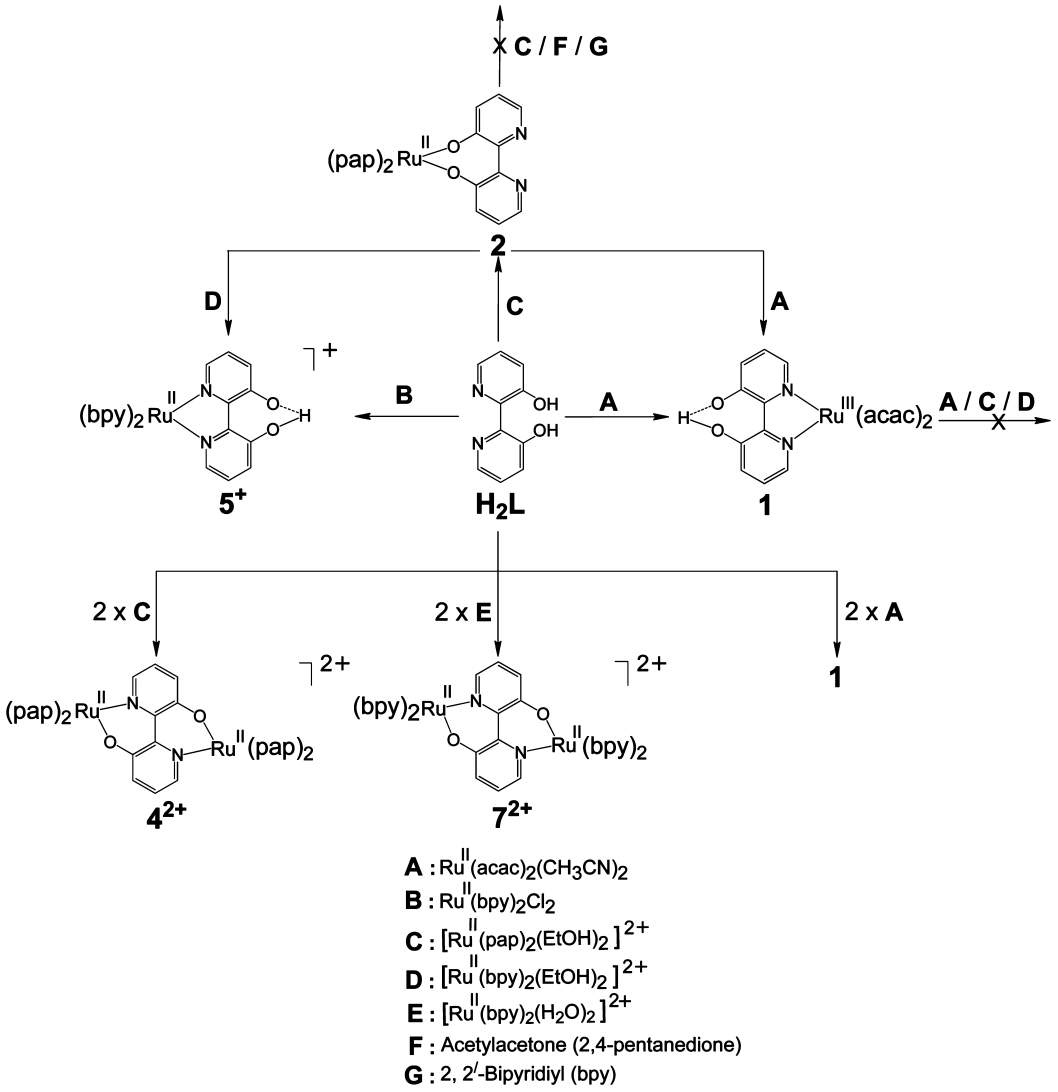

the binding of electron-rich O^-,O^- donating L^{2-} to the Ru(II) ion in spite of the less favorable seven-membered chelate situation. Thus, the collective consequence of the electronic aspect of the metal precursors ($\{Ru(acac)_2\}$, $\{Ru(bpy)_2\}$, $\{Ru(pap)_2\}$) and the chelate ring size (five-membered versus seven-membered) influences the preferential coordination mode of H_2L in **1**, **2**, and $[\mathbf{5}]PF_6$.

To further evaluate the prevailing electronic demand over the chelate constraint in **2**, the metal precursors $Ru(acac)_2(CH_3CN)_2$ and $[Ru(pap)_2(EtOH)_2]^{2+}$ were also reacted with the model 2,2′-biphenol (H_2L') ligand in the presence of NEt_3 as the base. Though H_2L' has altogether failed to bind with $\{Ru(acac)_2^{2+}\}$, it spontaneously reacts with $\{Ru(pap)_2^{2+}\}$ to give $Ru(pap)_2(L'^{2-})$ (**3**) (Scheme 2). The crystal structure of **3** (see below) establishes that the available O^-,O^- donors of L'^{2-} develop the seven-membered chelate ring as in **2**. Note that the corresponding $Ru^{II}(bpy)_2(L'^{2-})$ complex (**6**) is also reported.[1b] It thus implies that, under an optional condition of either the O^-,O^- (seven-membered chelate) or N,N (five-membered chelate) coordination mode of H_2L, the $\{Ru(bpy)_2\}$ fragment in $[\mathbf{5}]PF_6$ prefers the favorable five-membered N,N chelate situation, as was the case in **1** encompassing electron-donating $acac^-$ coligand. The relatively less π-accepting bpy[11,16] in $[\mathbf{5}]PF_6$ does not reduce the electron density on the metal ion to the extent that pap does in **2**, which in turn imposes the usual N,N binding mode of HL^- with favorable five-membered chelate ring in the former complex instead of the electron-rich O^-,O^- bonded strained seven-membered chelate ring as in the latter complex (Scheme 3).

Further, the reaction of **2** incorporating two suitably disposed free nitrogen donors in the backbone of coordinated L^{2-} with equimolar or excess $[Ru(pap)_2(EtOH)_2]^{2+}$ in refluxing ethanol failed to take place. The nonplanarity of two rings of the coordinated O^-,O^- bonded L^{2-} (see later) enhances the nonbonded N,N distance (2.831 Å) at the back face as compared to that of N,N bonded HL^- in **1** (2.579 Å), which in effect retards the binding of **2** with the second metal fragment ($\{Ru(pap)_2\}$ or $\{Ru(bpy)_2\}$ or $\{Ru(acac)_2\}$) (Scheme 3). However, to our surprise, the reaction of **2** with equimolar/excess $[Ru(bpy)_2(EtOH)_2]^{2+}$ or $Ru(acac)_2(CH_3CN)_2$ in refluxing ethanol results in the usual N,N bonded $\mathbf{5}^+$ or **1**, respectively, (Scheme 3) simply by eliminating the $\{Ru(pap)_2\}$ fragment from **2**, as revealed by their mass, absorption, and ^1H NMR spectral data. This further demonstrates the built-in structural constraint in **2** due to the seven-membered chelate ring involving L^{2-}. On the other hand, the free ligand, bpy or

dx.doi.org/10.1021/ic5004676 | Inorg. Chem. 2014, 53, 6094−6106

2,4-pentanedione, has failed to replace the pap ligand in **2**. The available hydrogen-bonded oxygen donors (O−H···O) in **1** also fail to react with $\{Ru(acac)_2\}$, $\{Ru(pap)_2\}$, or $\{Ru(bpy)_2\}$ (Scheme 3) primarily due to the stronger hydrogen-bonding effect (see later). This indeed has restrained us in achieving the unrecognized asymmetric bridging mode of L^{2-} (N,N and O^-,O^- donors, (**e**) in Scheme 1).

Dinuclear Complex [4](ClO$_4$)$_2$. The reaction of $[Ru(pap)_2(EtOH)_2]^{2+}$ with the H_2L ligand in 2:1 ratio and in the presence of NEt_3 base results in a dimeric complex $[(pap)_2Ru^{II}(\mu\text{-}L^{2-})Ru^{II}(pap)_2](ClO_4)_2$ ($[\mathbf{4}](ClO_4)_2$) (Scheme 2). The single-crystal X-ray structure of $[\mathbf{4}](ClO_4)_2$ reveals the symmetric ($N,O^-/N,O^-$) binding mode of the doubly deprotonated and twisted L^{2-} (see later) that has been reported for the analogous bpy complex $[(bpy)_2Ru^{II}(\mu\text{-}L^{2-})Ru^{II}(bpy)_2](PF_6)_2$ ($[\mathbf{7}](PF_6)_2$).[1a] On the other hand, $\{Ru(acac)_2\}$ failed to yield any dimeric species; it always leads to the formation of monomeric **1**, irrespective of $\{Ru(acac)_2\}-H_2L$ ratio (Scheme 3).

General Characterization. The newly synthesized paramagnetic **1** and diamagnetic **2**, **3**, and $[\mathbf{4}](ClO_4)_2$ complexes were characterized by standard analytical techniques. These complexes exhibit satisfactory microanalytical, conductivity, and mass spectral data (Figure S1, Supporting Information and Experimental Section). The $\nu(ClO_4)$ vibrations of $[\mathbf{4}](ClO_4)_2$ appear at 1100 and 625 cm^{-1}. The paramagnetic complex $Ru^{III}(acac)_2(HL^-)$ (**1**) exhibits magnetic moment corresponding to one unpaired electron (μ = 1.83 μ_B)[17] and rhombic electron paramagnetic resonance (EPR) spectrum, typical of Ru^{III} ion (t_{2g}^5, S = 1/2) in a distorted octahedral environment (see later).

Structural Aspects. The identities of **1**, **2**, **3**, and $[\mathbf{4}](ClO_4)_2$ were authenticated by their single-crystal X-ray structures (Figures 1−4, Tables 1 and 2, and Supporting Information,

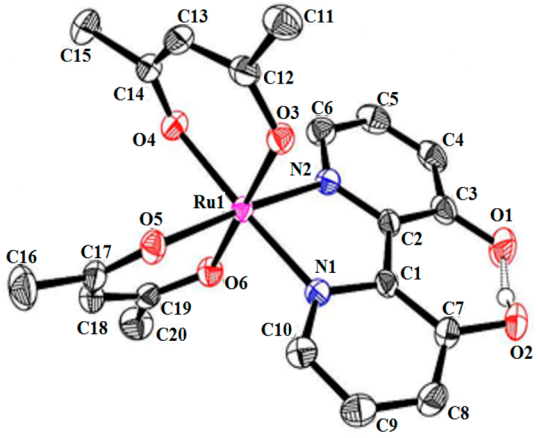

Figure 1. ORTEP diagram of **1**. Ellipsoids are drawn at 50% probability level. Hydrogen atoms are omitted for clarity.

Tables S1 and S2). The DFT-calculated bond parameters based on the optimized structures (Figure S2, Supporting Information) synchronize well with the experimental data.

The ligand HL^- in **1** is coordinated to the metal ion selectively through the N,N donors, forming a five-membered chelate ring (Figure 1). One of the pendant hydroxyl groups of H_2L is in a deprotonated state, its oxygen being hydrogen-bonded to the other OH group. The O2−H(101)/O1···H(101)/O1···O2 distances and O1···H101−O2 angle of

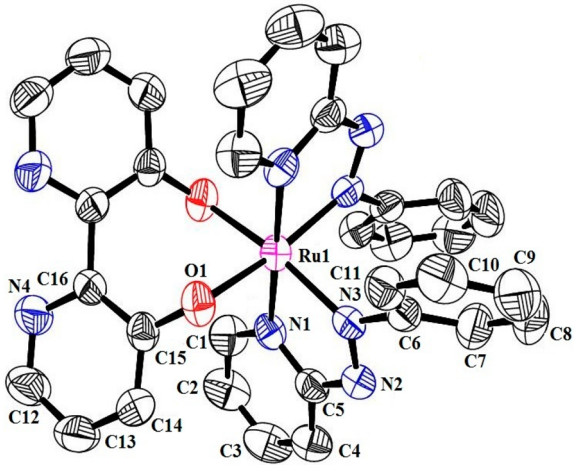

Figure 2. ORTEP diagram of **2**. Ellipsoids are drawn at 50% probability level. Hydrogen atoms and solvent molecule are omitted for clarity.

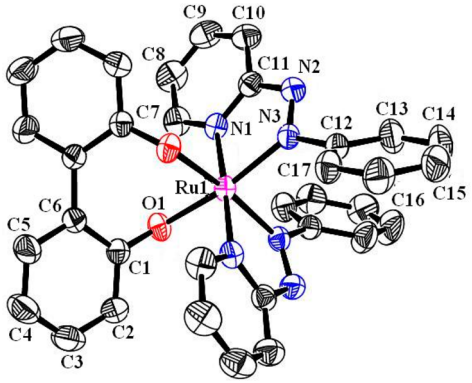

Figure 3. ORTEP diagram of **3**. Ellipsoids are drawn at 50% probability level. Hydrogen atoms are omitted for clarity.

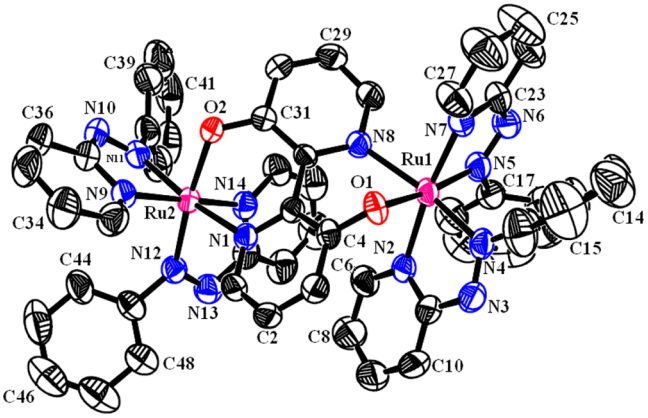

Figure 4. ORTEP diagram of the cation of $[\mathbf{4}](ClO_4)_2$. Ellipsoids are drawn at 50% probability level. Hydrogen atoms and solvent molecules are omitted for clarity.

0.85(5) Å/1.564 Å/2.38 Å and 166.64°, respectively, imply very strong hydrogen-bonding interaction.[18] The torsion angle N1−C1−C2−N2 of 6.00(3)° establishes the almost planar configuration of HL^- in **1**. The single bond length of C1−C2 associated with the connecting two rings of HL^- in **1** of 1.475(3) Å matches well with that reported for $\{Ru(bpy)_2\}$ complexes incorporating 4,4′-bpy$(OH)_2$/4,4′-bpy$(O^-)_2$[19a] and

dx.doi.org/10.1021/ic5004676 | Inorg. Chem. 2014, 53, 6094−6106

Table 1. Selected Crystallographic Parameters for 1, 2·H_2O, 3, and [4]$(ClO_4)_2$·C_7H_8·$2H_2O$

	1	2·H_2O	3	[4]$(ClO_4)_2$·C_7H_8·$2H_2O$
empirical formula	$C_{25}H_{21}N_2O_6Ru$	$C_{32}H_{26}N_8O_3Ru$	$C_{34}H_{26}N_6O_2Ru$	$C_{61}H_{54}Cl_2N_{14}O_{14}Ru_2$
formula weight	486.46	671.66	651.68	1480.19
crystal system	tetragonal	monoclinic	monoclinic	monoclinic
space group	$I\bar{4}$	$C2/c$	$I2/a$	$I2/a$
a (Å)	19.621 50(10)	18.758(5)	13.9060(2)	25.9006(5)
b (Å)	19.621 50(10)	13.8947(16)	13.3467(2)	14.5163(3)
c (Å)	12.171 10(10)	15.663(4)	16.1560(2)	34.5710(8)
α (deg)	90	90	90	90
β (deg)	90	133.66(4)	101.7970(10)	103.525(2)
γ (deg)	90	90	90	90
V (Å^3)	4685.91(5)	2953.5(11)	2935.21(7)	12637.6(5)
Z	8	4	4	8
μ (mm^{-1})	5.793	0.579	0.576	0.635
T (K)	150(2)	150(2)	150(2)	150(2)
D_{calcd} (g cm^{-3})	1.549	1.506	1.475	1.518
$F(000)$	2216	1360	1328	5856
2θ range (deg)	3.19 to 72.01	3.00 to 24.99	2.99 to 25.00	2.94 to 25.00
data/restraints/parameters	4573/0/270	2598/0/200	2575/0/ 195	11132/61/783
$R1$, $wR2$ [$I > 2\sigma(I)$]	0.0208, 0.0578	0.0451, 0.1157	0.0239, 0.0675	0.0631, 0.1592
$R1$, $wR2$(all data)	0.0209, 0.0579	0.0533,0.1254	0.0249, 0.0686	0.0916, 0.1858
GOF	1.063	1.123	1.058	1.056
largest diff. peak/hole, (e Å^{-3})	0.261 and −0.568	0.806 and −0.428	0.970 and −0.267	1.148 and −0.549

Table 2. Experimental and DFT-Calculated Selected Bond Lengths (Å) for 1, 2·H_2O, 3, and [4]$(ClO_4)_2$·C_7H_8·$2H_2O$

1			2·H_2O			3			[4]$(ClO_4)_2$ ·C_7H_8·$2H_2O$		
bond lengths (Å)	X-ray	DFT	bond lengths (Å)	X-ray	DFT	bond lengths (Å)	X-ray	DFT	bond lengths (Å)	X-ray	DFT
Ru1−N1	2.0275(18)	2.059	Ru1−O1	2.048(3)	2.057	Ru1−O1	2.0307(14)	2.054	Ru1−N4	1.978(5)	2.066
Ru1−N2	2.0320(19)	2.057	Ru1−N1	2.040(4)	2.072	Ru1−N1	2.0355(19)	2.064	Ru1−N5	1.988(5)	2.093
Ru1−O3	2.0001(16)	2.036	Ru1−N3	1.980(3)	2.060	Ru1 -N3	1.9887(17)	2.071	Ru1−N7	2.033(5)	2.074
Ru1−O4	2.0241(17)	2.078	N2−N3	1.305(5)	1.291	N2−N3	1.303(3)	1.291	Ru1−O1	2.049(4)	2.060
Ru1−O5	2.0277(16)	2.080	O1−C15	1.339(5)	1.337	O1−C1	1.338(2)	1.341	Ru1−N2	2.082(5)	2.101
Ru1−O6	2.0003(16)	2.037	C(16)−C(16)#1	1.505(8)	1.497	C6−C6#1	1.497(4)	1.488	Ru1−N8	2.134(5)	2.192
C3−O1	1.323(3)	1.284							Ru2−N11	1.983(5)	2.065
C7−O2	1.313(3)	1.310							Ru2−N12	1.984(5)	2.051
C1−C2	1.475(3)	1.474							Ru2−O2	2.037(4)	2.059
O2−H101	0.85(5)	1.096							Ru2−N9	2.051(5)	2.115
O1···H101	1.564	1.313							Ru2−N14	2.053(5)	2.091
									Ru2−N1	2.118(4)	2.181
									C5−C32	1.477(7)	1.488
									N3−N4	1.280(7)	1.279
									N10−N11	1.289(7)	1.276
									N12−N13	1.301(7)	1.291
									N5−N6	1.290(7)	1.287
									O1−C4	1.326(6)	1.308
									O2−C31	1.307(6)	1.304
									Ru1···Ru2	6.040	6.383

6,6′-bpy$(OH)_2$/6,6′-bpy$(O^-)_2$ (1.472(4) Å −1.483(4) Å).[19b] The C−O bond lengths (C3−O1 = 1.323(3) Å and C7−O2 = 1.313(3) Å) of mono deprotonated HL^- in **1** are in the midway of those reported for the {Ru$(bpy)_2$} complexes of protonated 4,4′-bpy$(OH)_2$/6,6′-bpy$(OH)_2$ (1.335(3) Å,1.343(3) Å /1.329(4) Å,1.340(5) Å) and doubly deprotonated 4,4′-bpy$(O^-)_2$/6,6′-bpy$(O^-)_2$ (1.294(3) Å,1.283(3) Å /1.248(3) Å,1.251(3) Å).[19] The average Ru−O(acac$^-$) and Ru−N(HL^-) bond distances of 2.0131(16) Å and 2.0297(18) Å, respectively, match well with the reported analogous complexes incorporating {$Ru^{III}(acac)_2$}[12c,20] and {$Ru^{III}(bpy)_2$}[21] metal fragments. The chelate bite angles involving acac ligands are close to 90° (O3−Ru1−O4, 91.96(7)°; O5−Ru1−O6, 91.55(7)°), whereas the same pertaining to the HL^- (N1−Ru1−N2) ligand is rather low (78.88(8)°), suggesting a distorted octahedral situation around the metal ion. Accordingly, the *trans* angles O3−Ru1−O6, O4−Ru1−N1, and O5−Ru1−N2 of 178.57(7)°, 177.04(7)°, and 175.97(7)°, respectively, deviate slightly form the ideal 180°.

The doubly deprotonated ligand L^{2-} or L'^{2-} in **2** or **3**, respectively, (Figures 2 and 3) is coordinated to the metal ion through the O^-,O^- donors, forming a seven-membered chelate ring. The *tc* configuration (*tc* = *trans* and *cis* with respect to the pyridine and azo nitrogens of pap ligands, respectively[11]) of the

dx.doi.org/10.1021/ic5004676 | Inorg. Chem. 2014, 53, 6094−6106

precursor {Ru(pap)$_2$} fragment was retained in **2** or **3**. The bite angles involving pap/L^{2-} in **2** (N1−Ru1−N3 = 76.65(13)°/O1−Ru1−O1#1 = 86.96(15)° and pap/L'^{2-} in **3** (N1−Ru1−N3 = 76.27(7)°/O1−Ru1−O1#1 = 87.48(8)°) imply distorted octahedral arrangements around the metal ions.

The nonplanarity of the two rings of L^{2-} and L'^{2-} in **2** and **3** are evidenced through the torsion angles of 51.20° (C15−C16−C16#1−C15#1) and 51.5° (C1−C6−C6#1−C1#1), respectively, as has also been reported for the $Ru^{II}(bpy)_2(L'^{2-})$ (**6**) of 58.5°.[1b] The Ru1−N3 (azo, pap) distances of 1.980(3) Å/1.9887(17) Å are appreciably shorter than Ru1−N1 (pyridine, pap) distances of 2.041(4) Å/ 2.0355(19) Å in **2** and **3**, respectively, due to strong (dπ)Ru^{II} → (π^*)N═N(pap) back-bonding effect.[15] The (dπ)Ru^{II} → (π^*)(N═N, pap) back-bonding effect has further been evidenced by the appreciable lengthening of the N═N bond of the coordinated pap ligand (N2−N3 = 1.305(5) Å and 1.303(3) Å in **2** and **3**, respectively) as compared to that reported for the free ligand (1.258(5) Å).[22]

The doubly deprotonated L^{2-} in [**4**]$(ClO_4)_2$ bridges the two {Ru(pap)$_2$} units symmetrically via the mixed N,O^- donors at each end, where Ru ions are separated by 6.040 Å (Figure 4). The *tc* configuration of the precursor {Ru(pap)$_2$} is maintained in the termini of [**4**]$(ClO_4)_2$ as in mononuclear **2** and **3**. The chelate bite angles involving pap (N2−Ru1−N4 (76.7(2)°), N5−Ru1−N7 (76.6(2)°), N9−Ru2−N11 (76.4(2)°), N12−Ru2−N14 (98.8(2)°) and L^{2-} (O1−Ru1−N8 (81.54(16)°), O2−Ru2−N1 (89.16(16)°) as well as interligand *trans* angles (O1−Ru1−N5 (170.49(19)°), N2−Ru1−N7 (171.55(19)°), N4−Ru1−N8 (167.72(18)°), O2−Ru2−N12 (173.70(17)°), N1−Ru2−N11 (167.3(2)°), N9−Ru2−N14 (174.45(19)°) define the distorted octahedral arrangement around each metal ion. The strong (dπ)Ru^{II} → (π^*)(N═N, pap) back-bonding in $\mathbf{4}^{2+}$ has been reflected in shorter Ru−N (azo, pap) distances (Ru1−N4/Ru1-N5, 1.978(5) Å/1.988(5) Å and Ru2−N11/Ru2-N12, 1.984(5) Å/1.984(5) Å) with respect to Ru−N(pyridine, pap) distances (Ru1−N2/Ru1−N7 2.082 Å/2.033(5) Å and Ru2−N9/Ru2−N14, 2.05(5) Å/2.053(5) Å) as well as lengthening of N═N(pap) distances (N3−N4/N5−N6, 1.287(7) Å/1.290(7) Å and N10−N11/N12−N13, 1.289(7) Å/1.301(7) Å) as in **2** or **3**. The Ru−N and Ru−O distances are in fairly good agreement with those in **1** and **2**, **3**, respectively. The nonplanarity of the bridge (L^{2-}) yields torsion angles C4−C5−C32−N8 and N1−C5−C32−C31 of 37.33° and 38.53°, respectively, which are, however, considerably smaller than that in O^-,O^- bonded L^{2-} in **2** (51.20°).

Spectral Aspects. The one-electron paramagnetic complex $Ru^{III}(acac^-)_2(HL^-)$ (**1**) exhibits a Ru(III)-based anisotropic EPR spectrum[23] in CH_3CN at 77 K (liquid nitrogen) with g_1 = 2.398, g_2 = 2.241, g_3 = 1.792, and $\langle g \rangle = ((1/3)(g_1^2 + g_2^2 + g_3^2))^{1/2}$ = 2.159, $\Delta g = g_1 - g_3$ = 0.61 (Figure 5).[24] The large Δg = 0.606 implies a distorted octahedral arrangement around the metal ion as has also been revealed by the molecular structure of **1**.

The ^{1}H NMR spectra of paramagnetic **1** and diamagnetic **2**, **3**, and $\mathbf{4}^{2+}$ are shown in Figure S3, Supporting Information, and chemical-shift values are listed in the Experimental Section. The paramagnetic complex **1** displays a well-resolved ^{1}H NMR spectrum over a large range of chemical shift (δ = +20 to −21 ppm) in $CDCl_3$, due to paramagnetic contact shift effect.[25] The four methyl groups and two CH protons of two acac ligands appear at −17.19 ppm, −20.28 ppm, and −3.92 ppm, respectively, due to internal symmetry. The peaks at 3.18 and

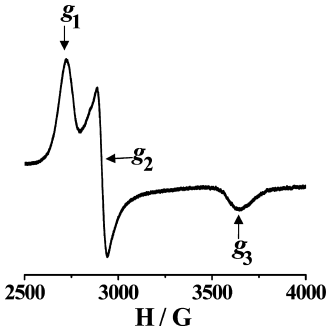

Figure 5. X-band EPR spectrum of **1** in CH_3CN at 77 K (liquid nitrogen).

19.30 ppm correspond to three aromatic protons and the hydrogen-bonded OH proton of the HL^- ligand, respectively. The diamagnetic monomeric (**2** and **3**) and dimeric ($\mathbf{4}^{2+}$) complexes exhibit partially overlapping 12, 13, and 21 aromatic proton resonances, respectively, within the chemical shift range (δ) of 9 to 5 ppm, corresponding to half of the molecule in each case due to internal symmetry.

The mixed-ligand complexes (**1**, **2**, **3**, and $\mathbf{4}^{2+}$) exhibit multiple moderately intense transitions in the visible (vis) region in addition to intense ligand-based bands in the higher-energy UV region in CH_3CN (Figure 6, Table 3). The vis

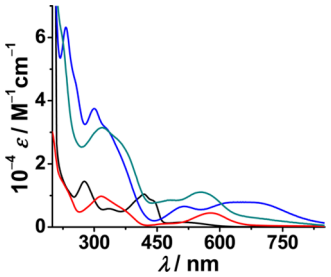

Figure 6. UV−vis spectra of **1** (black), **2** (red), **3** (blue), and [**4**]$(ClO_4)_2$ (green) in CH_3CN.

region transitions were assigned by TD-DFT calculations based on the optimized structure in each case (Table S3, Supporting Information). In the vis region, ruthenium(III) complex $Ru^{III}(acac)_2(HL^-)$ (**1**) exhibits one weak transition at 522 nm (ε/M^{-1} cm^{-1} = 1460) (DFT = 526 nm) followed by two close by moderately intense transitions at 440 nm (ε/M^{-1} cm^{-1} = 8410) (DFT = 423 nm) and 420 nm (ε/M^{-1} cm^{-1} = 10 390) (DFT = 346 nm) corresponding to mixed ligand/metal-derived charge-transfer bands of acac(π) → Ru(dπ), HL(π) → Ru(dπ), Ru(dπ)/HL(π) → HL(π^*)/acac(π^*), and HL(π)/Ru(dπ) → HL(π^*)/acac(π^*), respectively.[26] Similar mixing of metal−ligand orbitals in molecular orbitals (MOs) has also been reported in {Ru(bpy)$_2$} complexes of deprotonated 4,4′-dihydroxy-2,2′-bipyridine.[26f]

The pK_a value on protonation of **1**, that is, [Ru(acac)$_2$(H_2L)]$^+$, has been estimated via spectrophotometric titration in the pH range of 6−0.2 in 1:1.5 CH_3CN−H_2O mixture (as **1** is virtually insoluble in simple water). The plot of absorbance versus pH (Figure S4, Supporting Information) reveals the pK_a value to be ∼0.2. However, the possibility of pK_a even lower than that could not be ascertained since the lower limit in the pH electrode is 0.2. However, no change in spectral profile of **1** takes place in between pH 3−13.8,

dx.doi.org/10.1021/ic5004676 | Inorg. Chem. 2014, 53, 6094−6106

Table 3. UV−Vis Spectral Data of 1, 2, 3, and 4^{2+} in CH_3CN

complex	λ[nm] (ε[M^{-1} cm^{-1}])
1	276 (14 440), 338 (5760, sh), 420 (10 390), 440 (8410), 522 (1460)
2	230 (12 980, sh), 318 (9720), 368 (5990, sh), 465 (1090), 580 (4440)
3	232 (63 550), 301 (37 720), 334 (31 260, sh), 509 (6630), 662 (7470)
4^{2+}	222 (61 220, sh), 322 (30 910), 369 (25 890, sh), 478 (8910), 560 (11 670)

implying the stability of the hydrogen-bonded O−H···O form of the coordinated HL^- in **1**. The pK_a value of the analogous bpy derivative $[Ru(bpy)_2(HL^-)]^+$ ($\mathbf{5}^+$) in Scheme 3 was reported as 0.4 or less.[1a] These indeed reflect the strong O−H···O hydrogen-bonding interaction involving HL^- in **1** as has also been established by its solid-state crystal structure (Figure 1). This in essence justifies the inability of **1** to participate in binding with the second metal fragment as depicted in Scheme 3.

The pap-derived ruthenium(II) complex $Ru^{II}(pap)_2(L^{2-})$ (**2**) exhibits two visible energy bands at 580 nm (ε/M^{-1} cm^{-1} = 4440) (DFT = 538 nm) and 465 nm (ε/M^{-1} cm^{-1} = 1090) (DFT = 419 nm), which originate via Ru(dπ)/pap(π) → pap(π^*) and L^{2-}(π)/Ru(dπ) → pap(π^*) transitions, respectively. The pap-derived other monomeric complex $Ru^{II}(pap)_2(L'^{2-})$ (**3**) exhibits one broad transition centered at 662 nm (ε/M^{-1} cm^{-1} = 7470) (DFT = 629 nm) followed by another band at 509 nm (ε/M^{-1} cm^{-1} = 6630) (DFT = 554 nm) in the vis region, which are attributed to the transitions of L'^{2-}(π)/Ru(dπ)/pap(π) → pap(π^*)/Ru(dπ) and L'^{2-}(π)/Ru(dπ) → pap(π^*)/Ru(dπ), respectively.[27] The dinuclear complex $[(pap)_2Ru^{II}(\mu\text{-}L^{2-})Ru^{II}(pap)_2](ClO_4)_2$ [**4**]$(ClO_4)_2$ displays two vis-region bands at 560 nm (ε/M^{-1} cm^{-1} = 11670) (DFT = 599 nm) and 478 nm (ε/M^{-1} cm^{-1} = 8910) (DFT = 495 nm) involving metal and pap-based orbitals toward the charge-transfer processes of Ru(dπ) → pap(π^*) and Ru(dπ)/pap(π) → pap(π^*). This sort of mixing of frontier orbitals of the metal ion and the ligand moieties (HL^-, L^{2-}, L'^{2-}) in the MOs is a reflection of covalency due to the noninnocent behavior of the ligands (see the Electrochemistry section below) as has been commonly featured in ruthenium quinonoid frameworks.[26,28]

Electrochemistry and Molecular Orbital Compositions. Complexes **1**, **2**, **3**, and [**4**]$(ClO_4)_2$ exhibit multiple redox processes in CH_3CN within the potential range of ±2.0 V versus saturated calomel electrode (SCE). The voltammograms are shown in Figure 7, and the potentials are listed in Table 4. Since most of the entities (Ru, pap, HL^-, L^{2-}, L'^{2-}) in the complexes (**1**, **2**, **3** and [**4**]$(ClO_4)_2$) are potential redox noninnocent centers, it is therefore imperative to understand the involvement of the orbitals toward the observed redox processes. Unfortunately, electrochemically (coulometrically) generated redox states in each case are found to be unstable primarily due to their irreversible or quasi-reversible features even at the relatively faster cyclic voltammetric time scale. This indeed has precluded their further experimental assessment. However, varying electronic structural forms of $\mathbf{1}^n$-$\mathbf{4}^n$ (Figure 7, Table 4) have been predicted by DFT calculated MO compositions in all the redox states (Table 5 and Tables S4−S23, Supporting Information) in combination with Mulliken spin density distributions in paramagnetic states (Figure 8, Table 6 and Figure S5, Supporting Information) (see Scheme 4).

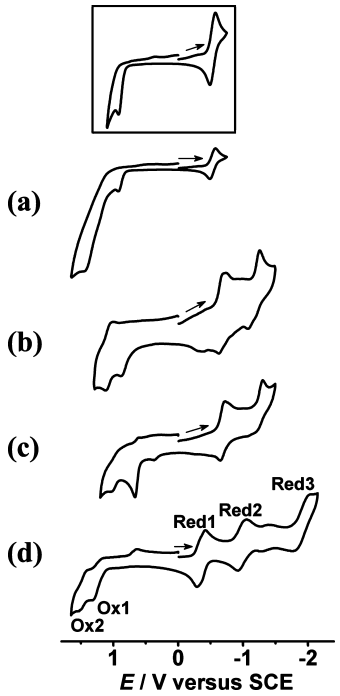

Figure 7. Cyclic voltammograms of (a) **1** (inset shows the Ox1 and Red1 only), (b) **2**, (c) **3** and (d) [**4**]$(ClO_4)_2$ in CH_3CN.

The complex $Ru^{III}(acac)_2(HL^-)$ (**1**) exhibits two irreversible oxidations at 0.92 V (Ox1) and 1.47 V (Ox2) and one reversible reduction at −0.53 V (Red1) (Figure 7a, Table 4).

Since both Ru^{III} and HL^- can in principle participate in oxidation processes,[29,10a,1a] the preferential involvement of metal-, ligand-, or mixed metal−ligand-based oribatals in the redox processes was, therefore, predicted by the MO compositions in different states. The MO compositions of **1**, $\mathbf{1}^+$, and $\mathbf{1}^{2+}$ (Table 5, Tables S4−S6, Supporting Information) suggest ligand-based first oxidation followed by metal-based second oxidation processes, leading to electronic structural forms of $[Ru^{III}(acac)_2(HL^{\bullet})]^+$ for $\mathbf{1}^+$ (Ox1) and $[Ru^{IV}(acac)_2(HL^{\bullet})]^{2+}$ for $\mathbf{1}^{2+}$ (Ox2) (Scheme 4). The assignments were also well-endorsed by the spin-density distributions in the paramagnetic states **1**, $\mathbf{1}^+$, and $\mathbf{1}^{2+}$ (Figure 8 and Table 6). The appreciable involvement of electron rich "$acac^-$" coligand in the spin accumulation processes in **1**, $\mathbf{1}^+$ and $\mathbf{1}^{2+}$ has also been noted recently for the analogous $\{Ru(acac)_2\}$ derived frameworks.[30] The ligand (HL^- → $HL^{\bullet}$) based oxidation in $[Ru^{II}(bpy)_2(HL^-)]^+$ ($\mathbf{5}^+$) is reported at 1.02 V versus SCE.[1a]

Note that the irreversible feature of the voltammograms for the oxidized $\mathbf{1}^+$ (Ox1) and $\mathbf{1}^{2+}$ (Ox2) (Figure 7a, Table 4) also suggests the possible ligand dissociation/complex decomposition on electron-transfer processes. Therefore, the DFT-supported electronic structural forms of $\mathbf{1}^+$ and $\mathbf{1}^{2+}$ as depicted in Scheme 4 need to be considered with appropriate caution.

On the other hand, the metal-based reduction $[Ru^{III}(acac)_2(HL^-)]$ (**1**) → $[Ru^{II}(acac)_2(HL^-)]^-$ ($\mathbf{1}^-$, Red1)

dx.doi.org/10.1021/ic5004676 | Inorg. Chem. 2014, 53, 6094−6106

Table 4. Redox Potentials and Comproportionation Constants

	$E°_{298}$/V (ΔE/mV)[c]					K_c[d]			
complexes	Ox2	Ox1	Red1	Red2	Red3	K_{c1}[d]	K_{c2}[d]	K_{c3}[d]	reference
1[a]	1.47[e]	0.92[e]	−0.53 (80)	-	-	2.09×10^9	-	-	this work
2[a]	1.05 (100)	0.86[e]	−0.67 (90)	−1.16 (160)	-	1.66×10^3	2.02×10^8	-	this work
3[a]	0.94 (190)	0.64[e]	−0.68 (80)	−1.21 (160)	-	1.21×10^5	9.61×10^8	-	this work
$\mathbf{4}^{2+}$[a]	1.46 (100)	1.24 (140)	−0.35 (130)	−0.99 (130)	−1.88 (200)	5.35×10^3	7.03×10^{10}	1.21×10^{15}	this work
$\mathbf{5}^{+}$[b]	1.38	1.02[e]	−1.45	−1.67	−2.24	1.26×10^6	5.35×10^3	4.58×10^9	1a
6[b]	0.94[e]	−0.12	−1.76	-	-	9.24×10^{17}	-	-	1b
$\mathbf{7}^{2+}$[b]	0.66	0.50	−1.55	−1.82	−1.88	5.15×10^2	3.77×10^4	10.39	1a

[a]Cyclic voltammetry in CH_3CN/0.1 M Et_4NClO_4, scan rate 100 mV s^{-1} [b]Cyclic voltammetry in CH_3CN/0.1 M $[NBu_4][PF_6]$ [c]Potential in V versus SCE; peak potential differences ΔE_p /mV (in parentheses). [d]Comproportionation constant from $RT \ln K_c = nF(\Delta E)$. K_{c1} between Ox1 and Ox2. K_{c2} between Red1 and Red2. K_{c3} between Red2 and Red3. [e]Irreversible process.

Table 5. DFT Calculated Selected MO Compositions for $\mathbf{1}^n$, $\mathbf{2}^n$, and $\mathbf{4}^n$

complex	MO	fragments	% contribution
1 (S = 1/2)	β-HOMO	HL	99
	β-LUMO	$Ru(acac)_2$	94
$\mathbf{1}^+$ (S = 1)	β-HOMO	$Ru(acac)_2$	88
	β-LUMO	HL	99
$\mathbf{1}^{2+}$ (S = 3/2)	β-HOMO	$Ru(acac)_2$	96
	β-LUMO	$Ru(acac)_2$	86
$\mathbf{1}^-$ (S = 0)	HOMO	$Ru(acac)_2$	95
2 (S = 0)	HOMO	L	86
	LUMO	pap	88
$\mathbf{2}^+$ (S = 1/2)	β-HOMO	$Ru(acac)_2$/ L	56/44
	β-LUMO	L	75
$\mathbf{2}^{2+}$ (S = 0)	LUMO	$Ru(acac)_2$ /L	26/74
$\mathbf{2}^-$ (S = 1/2)	SOMO	pap	89
	β-LUMO	pap	92
$\mathbf{2}^{2-}$ (S = 0)	HOMO	pap	94
$\mathbf{4}^{2+}$ (S = 0)	HOMO	Ru/L	20/66
$\mathbf{4}^{3+}$ (S = 1/2)	β-HOMO	Ru/L	56/27
	β-LUMO	Ru/L	32/55
$\mathbf{4}^{4+}$ (S = 1)	β-LUMO	Ru/L	62/22

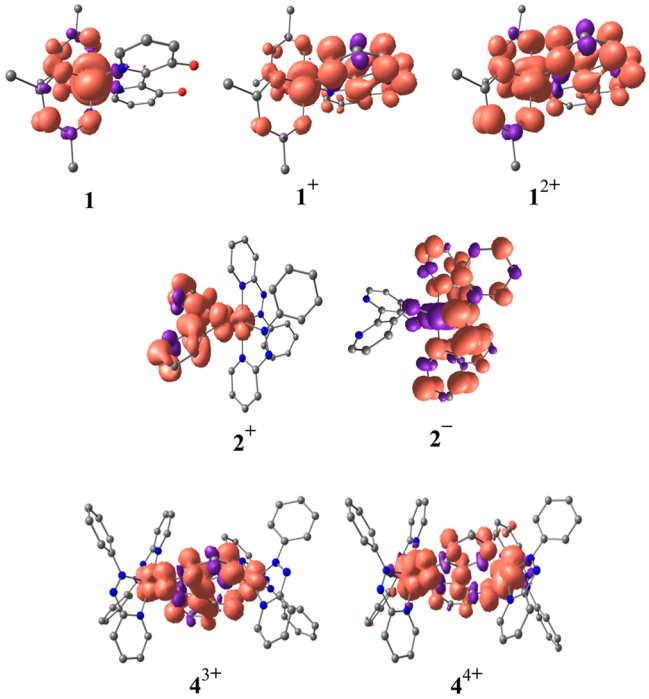

Figure 8. Mulliken spin-density plots of $\mathbf{1}^n$, $\mathbf{2}^n$, $\mathbf{3}^n$, and $\mathbf{4}^n$.

Table 6. DFT-Calculated Mulliken Spin Distributions for $\mathbf{1}^n$, $\mathbf{2}^n$, $\mathbf{3}^n$, and $\mathbf{4}^n$

complex	Ru	acac	pap	HL^-, L^{2-}, or L'^{2-}
1 (S = 1/2)	0.836	0.162		0.008
$\mathbf{1}^+$ (S = 1)	0.763	0.239		1.000
$\mathbf{1}^{2+}$ (S = 3/2)	1.202	0.727		1.067
$\mathbf{2}^+$ (S = 1/2)	0.086		−0.009	0.958
$\mathbf{2}^-$ (S = 1/2)	−0.354		1.398	−0.046
$\mathbf{3}^+$ (S = 1/2)	0.100		−0.017	0.915
$\mathbf{3}^-$ (S = 1/2)	−0.364		1.416	−0.046
$\mathbf{4}^{3+}$ (S = 1/2)	0.345		−0.032	0.690
$\mathbf{4}^{4+}$ (S = 1)	1.439		−0.004	0.562
$\mathbf{4}^+$ (S = 1/2)	−0.140		1.133	−0.018
4 (S = 1)	−0.394		2.432	−0.028
$\mathbf{4}^-$ (S = 3/2)	0.063		2.948	−0.004

(Scheme 4) instead of the alternate ligand-centered reduction (HL^-) was validated by the MO compositions of **1** and $\mathbf{1}^-$ (Table 5, Tables S4, S7, Supporting Information). The huge negative shift of Ru(III) → Ru(II) potential (−0.53 V) with respect to the corresponding bpy complex $\mathbf{5}^+$ (1.38 V)[1a] is due to the influence of three negatively charged ligand moieties (two $acac^-$ and one HL^-) around the metal ion, which in effect stabilizes Ru^{III} state in **1**, particularly under aerobic reaction condition.[12]

The complex $Ru^{II}(pap)_2(L^{2-})$ (**2**) incorporating strongly π-acidic pap ligands and O^-,O^- bonded L^{2-} exhibits two successive close by oxidations at 0.86 V (Ox1) and 1.05 V (Ox2) (Figure 7b, Table 4). The ligand- and mixed metal−ligand-dominated MOs in **2**, $\mathbf{2}^+$, and $\mathbf{2}^{2+}$, respectively, (Table 5 and Tables S8−S10, Supporting Information) predict ligand-based first oxidation, $Ru^{II}(pap)_2(L^{2-})$ (**2**) → $[Ru^{II}(pap)_2(L^{\bullet-})]^+$ ($\mathbf{2}^+$, Ox1) followed by mixed ligand/metal-based second oxidation, $[Ru^{II}(pap)_2(L^{\bullet-})]^+$ ($\mathbf{2}^+$) → $[Ru^{II}(pap)_2(L^0)]^{2+}/[Ru^{III}(pap)_2(L^{\bullet-})]^{2+}$ ($\mathbf{2}^{2+}$, Ox2) (Scheme 4). The spin distribution in $\mathbf{2}^+$ (Figure 8, Table 6) is also in agreement with the ligand-based first oxidation process (Ox1). The pap(N═N)-based successive two reductions (Red1 and Red2, Figure 7b, Table 4)[31] were supported via the MO compositions of **2**, $\mathbf{2}^-$, and $\mathbf{2}^{2-}$ (Table 5 and Tables S8, S11−S12, Supporting Information). However, spin-density distribution in the paramagnetic intermediate $\mathbf{2}^-$ (Figure 8, Table 6) predicts an appreciable negative spin on the metal ion, which in turn suggests a mixed electronic structural form of $[Ru^{II}(pap)(pap^{\bullet-})(L^{2-})]^-$ (major)/$[Ru^{I}(pap)_2(L^{2-})]^-$ (minor) (Scheme

dx.doi.org/10.1021/ic5004676 | Inorg. Chem. 2014, 53, 6094−6106

Scheme 4. Electronic Structural Forms of 1^n–4^n. The Primary Forms are Shown in Bold Face

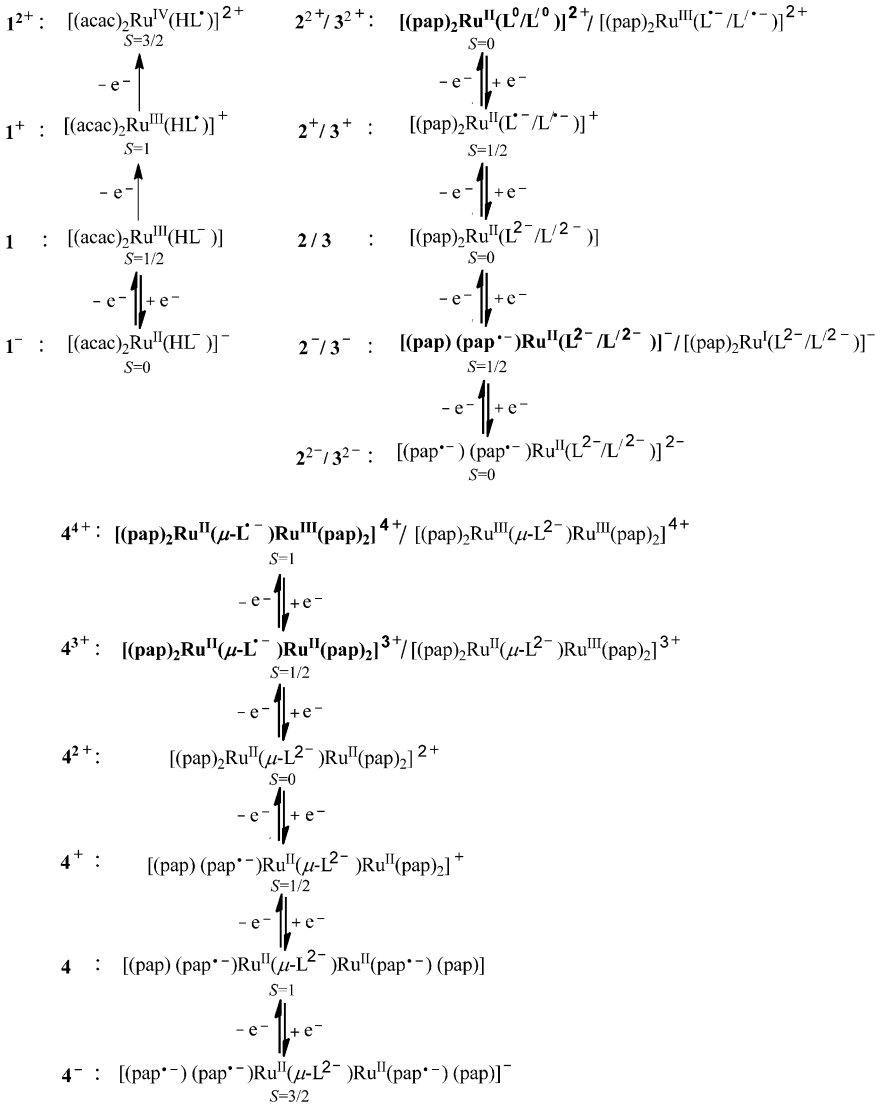

4).[30c] The positive shift (>1.5 V) of $Ru^{II}Ru^{III}$ potential on moving from $Ru^{III}(acac)_2(HL^-)$ (**1**) to $Ru^{II}(pap)_2(L^{2-})$ (**2**) is attributed to the specific electronic effect exerted by the pap ligand in the form of strong $(d\pi)Ru^{II} \rightarrow \pi^*(N{=}N, pap)$ back-bonding.[13] The strong back-bonding induced reduction of electron density on the metal ion essentially stabilizes the Ru(II) state even in the presence of dianionic L^{2-} state.[13]

Similar to **2**, the complex $Ru^{II}(pap)_2(L'^{2-})$ (**3**) exhibits two close by oxidations at 0.64 V (Ox1), 1.02 V (Ox2), and two successive reductions at −0.68 V (Red1), −1.21 V (Red2) (Figure 7c, Table 4). The MO compositions and spin-density distributions in $\mathbf{3}^n$ (n = +2, +1, 0, −1, −2) (Tables S13–S17, Supporting Information and Table 6, Figure S5, Supporting Information) are very close to those of respective $\mathbf{2}^n$, which, thus, suggest the ligand- and mixed ligand–metal-based Ox1 and Ox2, respectively, and mixed pap/Ru- and pap-based successive reductions (Scheme 4).

The dimeric complex $[(pap)_2Ru^{II}(\mu\text{-}L^{2-})Ru^{II}(pap)_2]^{2+}$ ($\mathbf{4}^{2+}$) exhibits two close by oxidation processes at 1.24 V (Ox1) and 1.46 V (Ox2) with a comproportionation constant (K_c) value of 5.3×10^3 ($RT \ln(K_c) = nF(\Delta E)$[32]) in addition to pap-based three successive reductions (Red1–Red3) in the potential range of −0.3 V to −2.0 V (Figure 7d, Table 4). The primarily ligand-based first oxidation process of $\mathbf{4}^{2+}$ was predicted by the MO contributions of $\mathbf{4}^{2+}$ and $\mathbf{4}^{3+}$ (Table 5 and Tables S18–S19, Supporting Information). The spin-density distribution in $\mathbf{4}^{3+}$ (Figure 8 and Table 6) also predicts L-dominated first oxidation process with partial involvement of the metal ion, leading to the electronic configuration of $[(pap)_2Ru^{II}(\mu\text{-}L^{\bullet -})Ru^{II}(pap)_2]^{3+}$ (major)/ $[(pap)_2Ru^{II}(\mu\text{-}L^{2-})\ Ru^{III}(pap)_2]^{3+}$ (minor) for $\mathbf{4}^{3+}$ (Scheme 4). The predominantly ligand (L)-based first oxidation potential of $\mathbf{4}^{2+}$ at 1.24 V is appreciably higher than that at 0.86 V in analogous mononuclear pap complex **2** due to the different binding modes of L^{2-} around each metal ion in the complexes, monoanionic N,O^- mode in $\mathbf{4}^{2+}$ versus dianionic O^-,O^- mode in **2** as well as additional electrostatic factor of the charge state in the latter. On the other hand, the MO compositions of $\mathbf{4}^{3+}$ and $\mathbf{4}^{4+}$ (Table 5 and Supporting Information, Tables S19 and S20) as well as Mulliken spin distributions in $\mathbf{4}^{4+}$ (Figure 8 and Table 6) suggest a metal-based second oxidation process $[(pap)_2Ru^{II}(\mu\text{-}L^{\bullet -})Ru^{III}(pap)_2]^{4+}$ with minor contribution from the alternate process of $[(pap)_2Ru^{III}(\mu\text{-}L^{2-})Ru^{III}(pap)_2]^{4+}$ (Scheme 4). Contrary to $\mathbf{4}^{2+}$, the close by two oxidation steps at 0.50 and 0.66 V versus SCE ($K_c = 5.1 \times 10^2$) for the reported bpy derivative $[(bpy)_2Ru^{II}(\mu\text{-}L^{2-})Ru^{II}(bpy)_2]^{2+}$ ($\mathbf{7}^{2+}$) are assigned

dx.doi.org/10.1021/ic5004676 | Inorg. Chem. 2014, 53, 6094–6106

to metal-based $Ru^{II}Ru^{II}/Ru^{II}Ru^{III}$ and $Ru^{II}Ru^{III}/Ru^{III}Ru^{III}$ processes, respectively, with the involvement of mixed-valent $Ru^{II}Ru^{III}$ intermediate.[1a] Thus, a substantial positive shift (~0.8 V) of Ru^{II}/Ru^{III} process occurs on substituting the ancillary ligand bpy in 7^{2+} by pap in 4^{2+} due to stronger π-acceptor character of pap. The 10-fold enhancement of K_c in 4^{3+} with respect to 7^{3+} in spite of stronger π-acceptor character of pap could be rationalized by the fact of preferential involvement of L^{2-} in the oxidation processes of the former complex. The similar difference in site-selective (ligand versus metal) oxidation process primarily based on pap and bpy coligands has also been reported recently in ligand-bridged diruthenium complexes: selective influence of pap facilitates the formation of phenoxyl radical bridged isovalent metal centers in $[(pap)_2Ru^{II}(\mu\text{-boptz}^{\bullet-})Ru^{II}(pap)_2]^{4+}$ ($boptz^{2-}$ = 3,6-bis(2-oxidophenyl)-1,2,4,5-tetrazine), while the corresponding bpy derivative develops the mixed-valent $Ru^{II}Ru^{III}$ state in $[(bpy)_2Ru^{II}(\mu\text{-boptz}^{2-})Ru^{III}(bpy)_2]^{3+}$.[33]

The pap-based successive reduction processes (Red1−Red3 in Figure 7d, Table 4) were established in the same way by the analysis of MO compositions in respective redox states (4^{2+}, 4^{+}, **4**, 4^{-}, Tables S18, S21−S23, Supporting Information) in combination with Mulliken spin-density plots in paramagnetic intermediates (Table 6, Scheme 4, and Supporting Information, Figure S5).

CONCLUSION

The unique influence of electronic features of the coligands (electron-rich $acac^{-}$, moderately π-acidic bpy, strongly π-acidic pap) in directing the different coordination modes of the ambidentate ligand 2,2′-bipyridine-3,3′-diol (H_2L) in a set of ruthenium complexes was evaluated. In $Ru^{III}(acac)_2(HL^{-})$ (**1**) and reported $[Ru^{II}(bpy)_2(HL^{-})]^{+}$ (5^{+}),[1a] the nearly planar HL^{-} develops the usual N,N bonded five-membered chelate with O−H···O hydrogen-bonding interaction at the backbone of the ligand framework. The strong O−H···O hydrogen-bonding interaction associated with the coordinated HL^{-} in **1** impedes its binding with the second metal fragment ({Ru(acac)$_2$} or {Ru(bpy)$_2$} or {Ru(pap)$_2$}). On the contrary, O^{-},O^{-} bonded seven-membered chelate with twisted L^{2-} was stabilized in $Ru^{II}(pap)_2(L^{2-})$ (**2**). The nonplanarity of L^{2-} in **2** prevents the binding of the second metal fragment ({Ru(pap)$_2$}, {Ru(bpy)$_2$}, or {Ru(acac)$_2$}) with the available N,N donors at its other face, which indeed restricts the formation of hitherto unrecognized unsymmetric bridging mode of L^{2-} (O^{-},O^{-}/N,N). The model ligand 2,2′-biphenolate (L'^{2-}), having the exclusive option of forming O^{-},O^{-} bonded seven-membered chelate, however, fails to make any such distinction with the electron-deficient metal centers in $[Ru^{II}(pap)_2(L'^{2-})]$ (**3**) and $[Ru^{II}(bpy)_2(L'^{2-})]$ (**6**), although L'^{2-} does not participate in reaction with the electron-rich metal fragment {Ru(acac)$_2$}. At the dinuclear level, L^{2-} extends the symmetric (N,O^{-}/N,O^{-}) bridging mode ({$Ru^{II}(\mu\text{-}L^{2-})Ru^{II}$}) with both the electron-deficient metal units, {$Ru(pap)_2^{2+}$} in 4^{2+} and {$Ru(bpy)_2^{2+}$} in 7^{2+};[1b] L^{2-} has, however, failed to bridge the {$Ru(acac)_2^{2+}$} fragments. The delicate balancing event between the electronic demand on the metal ion depending on the specific effect of coligands and the chelate size involving HL^{-} and L^{2-} has thus been instrumental in fine-tuning the eventual binding mode of H_2L in the complexes. Furthermore, DFT-calculated MO compositions and Mulliken spin-density plots reveal the effective participations of noninnocent HL^{-}, L^{2-}, L'^{2-}, and pap-based orbitals in addition to ruthenium ion in the accessible redox processes due to the built-in effect of covalency. Further studies with different metal precursors are in progress in stabilizing the currently unrecognized coordination modes of H_2L, that is, (**d**) and (**e**) in Scheme 1.

EXPERIMENTAL SECTION

Materials. The precursor metal complexes $Ru(acac)_2(CH_3CN)_2$[34] and *ctc*-$Ru(pap)_2Cl_2$[14a] and the ligand 2,2′-bipyridine-3,3′-diol (H_2L)[35] were prepared according to the reported procedures. The 2,2′-biphenol was purchased from Merck. All other chemicals and reagents were reagent grade, and for spectroscopic and electrochemical studies HPLC-grade solvents were used.

Physical Measurements. The electrical conductivities of the complexes in CH_3CN were checked with an Autoranging conductivity meter (Toshcon Industries, India). Fourier transform infrared (FT-IR) spectra were taken on a Nicolet spectrophotometer with samples prepared as KBr pellets. ^{1}H NMR spectra were recorded using a Bruker Advance III 400 MHz spectrometer. Cyclic voltammetry measurements were performed on a PAR model 273A electrochemistry system. Platinum wire working and auxiliary electrodes and a saturated calomel reference electrode (SCE) were used in a standard three-electrode configuration. A platinum wire-gauze working electrode was used for the constant potential coulometry experiment. Tetraethylammonium perchlorate (TEAP) was used as the supporting electrolyte, and concentration of the solution was taken as 10^{-3} M; the scan rate used was 100 mVs^{-1}. All electrochemical experiments were carried out under dinitrogen atmosphere. The half wave potential E°_{298} was set equal to $0.5(E_{pa} + E_{pc})$, where E_{pa} and E_{pc} are anodic and cathodic cyclic voltammetry peak potentials, respectively. The EPR measurements were made with a JEOL model FA200 electron spin resonance spectrometer. UV−vis spectral studies were performed on a PerkinElmer Lambda 950 spectrophotometer. The elemental analysis was carried out on a Thermoquest (EA 1112) micro analyzer. Electrospray mass spectra were recorded on a Bruker Microflex matrix-assisted laser desorption ionization time-of-flight (YA-105) mass spectrometer.

Synthesis of (acac)$_2$Ru(HL) (1). The precursor complex Ru(acac)$_2$(CH_3CN)$_2$ (50 mg, 0.131 mmol), ligand 2,2′-bipyridine-3,3′-diol (H_2L) (25 mg, 0.131 mmol), and triethylamine (20 mg, 0.197 mmol) (freshly distilled over KOH) were taken in 30 mL of ethanol. The mixture was refluxed under atmospheric conditions for 5 h. The initial light orange color of the reaction mixture gradually changed to deep reddish-brown. The solvent was removed under reduced pressure. The dried crude product was purified by using a silica gel (mesh size 60−120) column, which led to the elution of the red colored mononuclear complex **1** by the dichloromethane and acetonitrile (1:1) solvent mixture. Evaporation of the solvent under reduced pressure yielded the pure complex **1**, which was further dried under vacuum. Yield: 52 mg (82%). ^{1}H NMR in $CDCl_3$ [δ/ppm (J/Hz)]: 19.30 (s, broad, 1H), 3.18 (s, 6H), −3.77 (s, broad, 2H), −17.19 (s, broad, 6H), −20.28 (s, broad, 6H). MS (ESI+, MeCN): m/z {[MH]$^+$} calcd: 488.05; found: 488.04. Molar conductivity (MeCN): Λ_M = 6 Ω^{-1} cm^2 M^{-1}. Elemental analysis calcd (%) for $C_{20}H_{21}N_2O_6Ru$: C, 49.38; H, 4.35; N, 5.76. Found: C, 49.68; H, 4.28; N, 5.58.

Synthesis of (pap)$_2$Ru(L) (2). The precursor complex *ctc*-[(pap)$_2$$RuCl_2$] (50 mg, 0.093 mmol) in 25 mL of ethanol was refluxed with silver nitrate (47 mg, 0.279 mmol) for 2 h. The initial dark blue color of the reaction mixture gradually changed to deep reddish-violet. The precipitated AgCl was filtered off and washed with cold ethanol. The ligand 2,2′-bipyridine-3,3′-diol (H_2L) (18 mg, 0.093 mmol) was added to the filtrate and heated at reflux for 45 min under N_2 atmosphere. After that triethylamine (28 mg, 0.279 mmol) (freshly distilled over KOH) was added to the above hot solution. The initial reddish-violet color instantly changed to blue. The mixture was further heated to reflux under stirring conditions for 6 h under dinitrogen atmosphere. The solvent was removed under reduced pressure. The dried crude product was then purified by using a silica gel column (mesh size 60−120). The blue-colored mononuclear complex **2** was

dx.doi.org/10.1021/ic5004676 | Inorg. Chem. 2014, 53, 6094−6106

eluted by acetonitrile−methanol (10:1) mixture. Evaporation of the solvent under reduced pressure yielded the pure complex **2**, which was further dried under vacuum. Yield: 30 mg (50%). ^{1}H NMR in deuterated dimethyl sulfoxide (DMSO-d_6) [δ/ppm (J/Hz)]: 5.62 (d, 8.1, 1H), 6.50 (t, 8.1, 8.1, 1H), 6.76 (d, 8.0, 2H), 7.11 (t, 7.7, 7.7, 2H), 7.29 (t, 7.4, 7.4, 1H), 7.41 (t, 6.6, 6.6, 1H), 7.74 (d, 5.7, 1H), 8.08 (t, 7.7, 7.7, 1H), 8.32 (d, 5.8, 1H), 8.64 (d, 8.1, 1H).) MS (ESI+, MeCN): m/z {[MH]$^+$} calcd: 655.12; found: 655.11. Molar conductivity (MeCN): Λ_M = 3 Ω^{-1} cm^2 M^{-1}. Elemental analysis calcd (%) for $C_{32}H_{24}N_8O_2Ru$: C, 58.80; H, 3.70; N, 17.14; found: C, 58.53; H, 3.86; N, 17.31.

Synthesis of [(pap)$_2$Ru^{II}(L′)] (3). The mixture of complex *ctc*-[(pap)$_2$Ru^{II}Cl$_2$] (50 mg, 0.093 mmol) and silver nitrate (47 mg, 0.279 mmol) in 25 mL of ethanol was refluxed for 2 h. The initial dark blue color of the reaction mixture gradually changed to deep reddish-violet. The solution was allowed to cool at 298 K, and the precipitated AgCl was filtered off and washed with cold ethanol. The ligand 2,2′-biphenol (H_2L') (17 mg, 0.093 mmol) and triethylamine (28 mg, 0.279 mmol) were added to the filtrate, and the mixture was heated to reflux under dinitrogen atmosphere for 12 h; subsequently, the solvent was removed under reduced pressure. The crude product was purified by using a neutral alumina column, which led to the elution of the blue-colored complex **3** by dichloromethane. Evaporation of the solvent under reduced pressure yielded the pure complex **3**, which was further dried under vacuum. Yield: 55 mg (91%). ^{1}H NMR in $CDCl_3$ [δ/ppm (J/Hz)]: 5.38 (d, 7.92, 1H), 6.41 (t, 7.72, 7.52, 1H), 6.58 (t, 7.32, 7.32, 1H), 6.87 (d, 8.4, 2H), 6.94 (d, 7.3, 1H), 7.05 (t, 8.44, 7.48, 2H), 7.22 (m, 2H), 7.86 (t, 7.44, 8.08, 1H), 8.47 (d, 8.04, 1H), 8.69 (d, 6.64, 1H). MS (ESI+, MeCN): m/z {[MH]$^+$} calcd: 653.12; found: 653.08. Molar conductivity (MeCN): Λ_M = 4 Ω^{-1} cm^2 M^{-1}. Elemental analysis calcd (%) for $C_{34}H_{26}N_6O_2Ru$: C, 62.66; H, 4.02; N, 12.90; found: C, 62.75; H, 4.05; N, 12.74.

Synthesis of [(pap)$_2$Ru^{II}(μ-L)Ru^{II}(pap)$_2$)](ClO$_4$)$_2$ ([4](ClO$_4$)$_2$). *ctc*-[(pap)$_2$Ru^{II}Cl$_2$] (50 mg, 0.093 mmol) and silver nitrate (47 mg, 0.279 mmol) were taken in 25 mL of ethanol and heated to reflux for 2 h. The initial dark blue color of the reaction mixture gradually changed to deep reddish-violet. The solution was allowed to settle at 298 K, and the precipitated AgCl was filtered and washed with cold ethanol. The ligand 2,2′-bipyridine-3,3′-diol (H_2L) (35 mg, 0.186 mmol) and triethylamine (28 mg, 0.279 mmol) were added to the aforesaid filtrate. The reaction mixture was heated to reflux under dinitrogen atmosphere for 10 h. The solvent was removed, and the solid mass thus obtained was redissolved in 5 mL of acetonitrile. Saturated sodium perchlorate aqueous solution was added to the above solution, which led to the formation of dark solid. The solid mass was filtered off, washed thoroughly by ice-cooled water, and dried in vacuum. It was then purified by a silica gel (mesh 60−120) column, and the pure [**4**](ClO$_4$)$_2$ was eluted by 5:1 dichloromethane−acetonitrile mixture. The pure complex was further dried under vacuum. Yield: 49 mg (80%). ^{1}H NMR in CD_3CN [δ/ppm (J/Hz)]: 6.65 (d, 8.52, 2H), 6.76 (d, 5.04, 1H), 6.84 (m, 2H), 6.93 (d, 7.64, 2H) 6.97 (d, 8.12, 1H), 7.17 (t, 7.56, 7.52, 3H), 7.33 (m, 4H), 7.49 (t, 7.52, 7.44, 1H), 7.56 (d, 4.88, 1H), 8.15 (m, 2H), 8.64 (d, 8.00, 1H), 8.76 (d, 7.04, 1H). MS (ESI+, MeCN): m/z {[M − ClO$_4$]$^+$} calcd: 1221.12; found: 1221.11. Molar conductivity (MeCN): Λ_M = 230 Ω^{-1} cm^2 M^{-1}. IR (KBr): ν (ClO_4^-, cm^{-1}): 1100, 625. Elemental analysis calcd (%) for $C_{54}H_{42}Cl_2N_{14}O_{10}Ru_2$: C, 49.13; H, 3.21; N, 14.86; found, C, 49.27; H, 3.10; N, 14.61.

Crystal Structure Determination. Single crystals of **1**, **2**, **3**, and [**4**](ClO$_4$)$_2$ were grown by slow evaporation of their 1:1 dichloromethane−hexane, methanol, 1:1 dichloromethane−acetonitrile, and 1:1 dichloromethane−toluene solutions, respectively. X-ray crystal data were collected on a CCD Agilent Technologies (Oxford Diffraction) Super Nova diffractometer. Data collection was evaluated by using the CrysAlisPro CCD software. The data were collected by the standard φ-ω scan techniques and were scaled and reduced using CrysAlisPro RED software. The structure was solved by direct method using SHELXS-97 and refined by full matrix least-squares with SHELXL-97, refining on F^2.[36] All non-hydrogen atoms were refined anisotropically. The remaining hydrogen atoms were placed in geometrically constrained positions and refined with isotropic temperature factors, generally 1.2U_{eq} of their parent atoms. Hydrogen atoms were included in the refinement process as per the riding model. Hydrogen atoms associated with the solvent water molecules in **2** and [**4**](ClO$_4$)$_2$ could not be located; however, these were considered for the empirical formula in Table 1.

Computational Details. Full geometry optimizations were carried out by using the DFT method at the (R)B3LYP level for **1**$^-$, **2**, **2**$^{2+}$, **2**$^{2-}$, **3**, **3**$^{2+}$, **3**$^{2-}$, and **4**$^{2+}$ and at the (U)B3LYP level for **1**, **1**$^+$, **1**$^{2+}$, **2**$^+$, **2**$^-$, **3**$^+$, **3**$^-$, **4**$^{3+}$, **4**$^{4+}$, **4**$^+$, **4**, and **4**$^-$.[37] Except ruthenium all other elements were assigned the 6-31G* basis set. The LANL2DZ basis set with effective core potential was employed for the ruthenium atom.[38] The vibrational frequency calculations were performed to ensure that the optimized geometries represent the local minima, and there are only positive Eigen values. All calculations were performed with Gaussian09 program package.[39] Vertical electronic excitations based on (R)B3LYP/(U)B3LYP optimized geometries were computed for **1**^{n} (n = +2, +1, 0, −1), **2**^{n} (n = +2, +1, 0, −1, −2), **3**^{n} (n = +2, +1, 0, −1, −2), and **4**^{n} (n = +4, +3, +2, +1, 0, −1) using the TD-DFT formalism[40] in acetonitrile using conductor-like polarizable continuum model (CPCM).[41] Chemissian 1.7[42] was used to calculate the fractional contributions of various groups to each MO. All calculated structures were visualized with ChemCraft.[43]

■ ASSOCIATED CONTENT

Ⓢ Supporting Information

X-ray crystallographic files of **1** (CCDC No. 988667), **2** (CCDC No. 988668), **3** (CCDC No. 988669), and [**4**](ClO$_4$)$_2$ (CCDC No. 988670) in CIF format, DFT data set for **1**^{n}, **2**^{n}, **3**^{n}, and **4**^{n} (Tables S3−S23, Figures S2 and S5), bond angles (Tables S1 and S2), mass spectra (Figure S1), ^{1}H NMR spectra (Figure S3), UV−vis spectra of **1** as a function of pH (Figure S4). This material is available free of charge via the Internet at http://pubs.acs.org.

■ AUTHOR INFORMATION

Corresponding Author

*E-mail: lahiri@chem.iitb.ac.in. Phone: +91 22 25767159. Fax: +91 22 25723480.

Notes

The authors declare no competing financial interest.

■ ACKNOWLEDGMENTS

Financial support received from the Department of Science and Technology, Council of Scientific and Industrial Research (fellowships to P.G., P.M., and A.D.) and from the University Grants Commission (fellowship to R.R.), New Delhi (India), is gratefully acknowledged.

■ REFERENCES

(1) (a) Thompson, A. M. W. C.; Jeffery, J. C.; Liard, D. J.; Ward, M. D. *J. Chem. Soc., Dalton Trans.* **1996**, 879−884. (b) Laye, R. H.; Bell, Z. R.; Ward, M. D. *New J. Chem.* **2003**, *27*, 684−691.

(2) Bugarcic, T.; Habtemariam, A.; Stepankova, J.; Heringova, P.; Kasparkova, J.; Deeth, R. J.; Johnstone, R. D. L.; Prescimone, A.; Parkin, A.; Parsons, S.; Brabec, V.; Sadler, P. J. *Inorg. Chem.* **2008**, *47*, 11470−11486.

(3) (a) Li, H.; Hou, C.; Shi, J.-M.; Zhang, S.-G. *J. Coord. Chem.* **2008**, *61*, 3501−3507. (b) Hou, C.; Shi, J.-M.; Sun, Y.-M.; Shi, W.; Cheng, P.; Liu, L.-D. *Dalton Trans.* **2008**, 5970−5976. (c) Stephenson, M. D.; Hardie, M. J. *CrystEngComm.* **2007**, *9*, 496−502. (d) Jung, O.-S.; Kim, Y. T.; Lee, Y.-A.; Kim, Y. J.; Chae, H. K. *Inorg. Chem.* **1999**, *38*, 5457−5460.

(4) Himeda, Y.; Komatsuzaki, N. O.; Sugihara, H.; Kasuga, K. *Organometallics* **2007**, *26*, 702−712.

(5) Mendivil, E.-T.; Diez, J.; Cadierno, V. *Catal. Sci. Technol.* **2011**, *1*, 1605−1615.
(6) Zhang, S. G.; Hou, C. *Acta Crystallogr.* **2008**, *E64*, m1131.
(7) Li, M. J-. *J. Chem. Crystallogr.* **2009**, *39*, 143−146.
(8) Kunkely, H.; Vogler, A. *Inorg. Chim. Acta* **2003**, *343*, 357−360.
(9) (a) Giordino, P. J.; Bock, C. K.; Wrighton, M. S. *J. Am. Chem. Soc.* **1978**, *100*, 6960−6965. (b) Haga, M. *Inorg. Chim. Acta* **1983**, *75*, 29−35. (c) Kundu, T.; Mobin, S. M.; Lahiri, G. K. *Dalton Trans.* **2010**, *39*, 4232−4242. (d) Rakowski Dubois, M.; Dubois, D. L. *Chem. Soc. Rev.* **2009**, *38*, 62−72.
(10) (a) DesPasquale, J.; Nieto, I.; Reuther, L. E.; Herbst-Gervasoni, C. J.; Paul, J. J.; Mochalin, V.; Zeller, M.; Thomas, C. M.; Addison, A. W. *Inorg. Chem.* **2013**, *52*, 9175−9183. (b) Himeda, Y. *Eur. J. Inorg. Chem.* **2007**, 3927−3941.
(11) Lahiri, G. K.; Bhattacharya, S.; Goswami, S.; Chakravorty, A. *J. Chem. Soc., Dalton Trans.* **1990**, 561−565.
(12) (a) Patra, S.; Miller, T. A.; Sarkar, B.; Niemeyer, M.; Ward, M. D.; Lahiri, G. K. *Inorg. Chem.* **2003**, *42*, 4707−4713. (b) Patra, S.; Mondal, B.; Sarkar, B.; Niemeyer, M.; Lahiri, G. K. *Inorg. Chem.* **2003**, *42*, 1322−1327. (c) Ghumaan, S.; Kar, S.; Mobin, S. M.; Harish, B.; Puranik, V. G.; Lahiri, G. K. *Inorg. Chem.* **2006**, *45*, 2413−2423.
(13) Bag, N.; Pramanik, A.; Lahiri, G. K.; Chakravorty, A. *Inorg. Chem.* **1992**, *31*, 40−45.
(14) (a) Ohta, T.; Takaya, H.; Noyori, R. *Inorg. Chem.* **1988**, *27*, 566−569. (b) Alguindigue, S. S.; Khan, M. A.; Ashby, M. T. *Organometallics* **1999**, *18*, 5112−5119. (c) Singh, A.; Bharty, M. K.; Kushawaha, S. K.; Butcher, R. J.; Singh, N. K. *Polyhedron* **2011**, *30*, 1927−1934. (d) Kukushkin, Y. N.; Kiseleva, N. P.; Zangrando, E.; Kukushkin, V. Y. *Inorg. Chim. Acta* **1999**, *285*, 203−207.
(15) (a) Mondal, B.; Paul, H.; Puranik, V. G.; Lahiri, G. K. *J. Chem. Soc., Dalton Trans.* **2001**, 481−487. (b) Chanda, N.; Laye, R. H.; Chakraborty, S.; Paul, R. L.; Jeffery, J. C.; Ward, M. D.; Lahiri, G. K. *J. Chem. Soc., Dalton Trans.* **2002**, 3496−3504. (c) Ghumaan, S.; Mukherjee, S.; Kar, S.; Roy, D.; Mobin, S. M.; Sunoj, R. B.; Lahiri, G. K. *Eur. J. Inorg. Chem.* **2006**, 4426−4441.
(16) (a) Goswami, S.; Mukherjee, R.; Chakravorty, A. *Inorg. Chem.* **1983**, *22*, 2825−2832. (b) Toket-Takvoryan, N. E.; Hemingway, R. E.; Bard, A. J. *J. Am. Chem. Soc.* **1973**, *95*, 6582−6589. (c) Seddon, E. A.; Seddon, K. R. *The Chemistry of Ruthenium;* Elsevier: Amsterdam, 1984, ch. 8, p 155.
(17) (a) Bag, N.; Lahiri, G. K.; Bhattacharya, S.; Favello, L. R.; Chakravorty, A. *Inorg. Chem.* **1988**, *27*, 4396−4402. (b) Lahiri, G. K.; Bhattacharya, S.; Ghosh, B. K.; Chakravorty, A. *Inorg. Chem.* **1987**, *26*, 4324−4331. (c) Mondal, B.; Chakraborty, S.; Munshi, M.; Walawalkar, M. G.; Lahiri, G. K. *J. Chem. Soc., Dalton Trans.* **2000**, 2327−2335. (d) Das, A.; Kundu, T.; Mobin, S. M.; Priego, J. S.; Jiménez-Aparicio, R.; Lahiri, G. K. *Dalton Trans.* **2013**, *42*, 13733−13746.
(18) (a) Gilli, P.; Bertolasi, V.; Ferreti, V.; Gilli, G. *J. Am. Chem. Soc.* **1994**, *116*, 909−915. (b) Emsely, J. *Chem. Soc. Rev.* **1980**, *9*, 91−124. (c) Novak, A. *Struct. Bonding (Berlin, Ger.)* **1974**, *18*, 177−216. (d) Speakman, J. C. *Struct. Bonding (Berlin, Ger.)* **1974**, *12*, 141−199.
(19) (a) Klein, S.; Dougherty, W. G.; Kassel, W. S.; Dudley, T. J.; Paul, J. J. *Inorg. Chem.* **2011**, *50*, 2754−2763. (b) Hufziger, K. T.; Thowfeik, S. F.; Charboneau, D. J.; Nieto, I.; Dougherty, W. G.; Kassel, W. S.; Dudley, T. J.; Merino, E.; Papish, E. T.; Paul, J. J. *J. Inorg. Biochem.* **2014**, *130*, 103−111.
(20) (a) Matsuzawa, H.; Ohashi, Y.; Kaizu, Y.; Kobayashi, H. *Inorg. Chem.* **1988**, *27*, 2981−2985. (b) Kar, S.; Chandra, N.; Mobin, S. M.; Urbanos, F. A.; Niemeyer, M.; Puranik, V. G.; Jiménez-Aparicio, R.; Lahiri, G. K. *Inorg. Chem.* **2005**, *44*, 1571−1579. (c) Das, D.; Das, A. K.; Sarkar, B.; Mondal, T. K.; Mobin, S. M.; Zališ, S.; Urbanos, F. A.; Kaim, W.; Lahiri, G. K. *Inorg. Chem.* **2009**, *48*, 11853−11864.
(21) Gilbert, J. A.; Eggleston, D. S.; Murphy, W. R., Jr.; Geselowitz, D. A.; Gersten, S. W.; Hodgson, D. J.; Meyer, T. J. *J. Am. Chem. Soc.* **1985**, *107*, 3855−3864.
(22) Majumdar, P.; Peng, S.-M.; Goswami, S. *J. Chem. Soc., Dalton Trans.* **1998**, 1569−1574.
(23) (a) DeSimone, R. E. *J. Am. Chem. Soc.* **1973**, *95*, 6238−6244. (b) Das, D.; Sarkar, B.; Kumbhakar, D.; Mondal, T. K.; Mobin, S. M.; Fiedler, J.; Urbanos, F. A.; Jiménez-Aparicio, R.; Kaim, W.; Lahiri, G. K. *Chem.—Eur. J.* **2011**, *17*, 11030−11040. (c) Das, A.; Scherer, T. M.; Mondal, P.; Mobin, S. M.; Kaim, W.; Lahiri, G. K. *Chem.—Eur. J.* **2012**, *18*, 14434−14443.
(24) Patra, S.; Sarkar, B.; Mobin, S. M.; Kaim, W.; Lahiri, G. K. *Inorg. Chem.* **2003**, *42*, 6469−6473.
(25) (a) Koiwa, T.; Masuda, Y.; Shono, J.; Kawamoto, Y.; Hoshino, Y.; Hashimoto, T.; Natarajan, K.; Shimizu, K. *Inorg. Chem.* **2004**, *43*, 6215−6223. (b) Eaton, D. R. *J. Am. Chem. Soc.* **1965**, *87*, 3097−3102. (c) Palmer, R. A.; Fay, R. C.; Piper, T. S. *Inorg. Chem.* **1964**, *3*, 875−881. (d) Holm, R. H.; Cotton, F. A. *J. Am. Chem. Soc.* **1958**, *80*, 5658−5663. (e) Fay, R. C.; Piper, T. S. *J. Am. Chem. Soc.* **1963**, *85*, 500−504. (f) Chen, J.-L.; Zhang, X.-D.; Zhang, L.-Y.; Shi, L.-X.; Chen, Z.-N. *Inorg. Chem.* **2005**, *44*, 1037−1043. (g) Das, A.; Scherer, T.; Maji, S.; Mondal, T. K.; Mobin, S. M.; Urbanos, F. A.; Jiménez-Aparicio, R.; Kaim, W.; Lahiri, G. K. *Inorg. Chem.* **2011**, *50*, 7040−7049. (h) Kumbhakar, D.; Sarkar, B.; Maji, S.; Mobin, S. M.; Fiedler, J.; Urbanos, F. A.; Jiménez-Aparicio, R.; Kaim, W.; Lahiri, G. K. *J. Am. Chem. Soc.* **2008**, *130*, 17575−17583.
(26) (a) Daria, K.; Dares, C.; Kaluarachchi, H.; Potvin, P. G.; Lever, A. B. P. *Inorg. Chem.* **2008**, *47*, 10110−10126. (b) McKinnon, S. D. J.; Patrick, B. O.; Lever, A. B. P.; Hicks, R. G. *Chem. Commun.* **2010**, *46*, 773−775. (c) McKinnon, S. D. J.; Patrick, B. O.; Lever, A. B. P.; Hicks, R. G. *Inorg. Chem.* **2013**, *52*, 8053−8066. (d) Maji, S.; Sarkar, B.; Patra, S.; Fiedler, J.; Mobin, S. M.; Puranik, V. G.; Kaim, W.; Lahiri, G. K. *Inorg. Chem.* **2006**, *45*, 1316−1325. (e) Maji, S.; Sarkar, B.; Mobin, S. M.; Fiedler, J.; Urbanos, F. A.; Jiménez-Aparicio, R.; Kaim, W.; Lahiri, G. K. *Inorg. Chem.* **2008**, *47*, 5204−5211. (f) Ghumaan, S.; Sarkar, B.; Maji, S.; Puranik, V. G.; Fiedler, J.; Urbanos, F. A.; Jiménez-Aparicio, R.; Kaim, W.; Lahiri, G. K. *Chem.—Eur. J.* **2008**, *14*, 10816−10828. (g) Fuentes, M. J.; Bognanno, R. J.; Dougherty, W. G.; Boyko, W. J.; Kassel, W. S.; Dudley, T. J.; Paul, J. J. *Dalton Trans.* **2012**, *41*, 12514−12523.
(27) (a) Das, D.; Mondal, T. K.; Mobin, S. M.; Lahiri, G. K. *Inorg. Chem.* **2009**, *48*, 9800−9810. (b) Maji, S.; Sarkar, B.; Mobin, S. M.; Fiedler, J.; Kaim, W.; Lahiri, G. K. *Dalton Trans.* **2007**, 2411−2418.
(28) (a) Gorelsky, S. I.; Lever, A. B. P.; Ebadi, M. *Coord. Chem. Rev.* **2002**, *230*, 97−105. (b) Haga, M.; Dodsworth, E. S.; Lever, A. B. P. *Inorg. Chem.* **1986**, *25*, 447−453. (c) DelMedico, A.; Dodsworth, E. S.; Lever, A. B. P.; Pietro, W. J. *Inorg. Chem.* **2004**, *43*, 2654−2671. (d) Ward, M. D.; McCleverty, J. A. *J. Chem. Soc., Dalton Trans.* **2002**, 275−288.
(29) (a) Kar, S.; Sarkar, B.; Ghumaan, S.; Roy, D.; Urbanos, F. A.; Fiedler, J.; Sunoj, R. B.; Jiménez-Aparicio, R.; Kaim, W.; Lahiri, G. K. *Inorg. Chem.* **2005**, *44*, 8715−8722. (b) Kar, S.; Sarkar, B.; Ghumaan, S.; Janardanan, D.; van Slageren, J.; Fiedler, J.; Puranik, V. G.; Sunoj, R. B.; Kaim, W.; Lahiri, G. K. *Chem.—Eur. J.* **2005**, *11*, 4901−4911. (c) Zhang, T.; Wang, C.; Liu, S.; Wang, J.-L.; Lin, W. *J. Am. Chem. Soc.* **2014**, *136*, 273−281.
(30) (a) Das, A.; Scherer, T. M.; Mobin, S. M.; Kaim, W.; Lahiri, G. K. *Inorg. Chem.* **2012**, *51*, 4390−4397. (b) Das, A.; Ghosh, T. K.; Chowdhury, A. D.; Mobin, S. M.; Lahiri, G. K. *Polyhedron* **2013**, *52*, 1130−1137. (c) Agarwala, H.; Scherer, T. M.; Mobin, S. M.; Kaim, W.; Lahiri, G. K. *Dalton Trans.* **2014**, *43*, 3939−3948.
(31) (a) Santra, B. K.; Lahiri, G. K. *J. Chem. Soc., Dalton Trans.* **1997**, 129−136. (b) Goswami, S.; Chakravarty, A. R.; Chakravorty, A. *Inorg. Chem.* **1981**, *20*, 2246−2250.
(32) Creutz, C. *Prog. Inorg. Chem.* **1983**, *30*, 1−73.
(33) Patra, S.; Sarkar, B.; Maji, S.; Fiedler, J.; Urbanos, F. A.; Jiménez-Aparicio, R.; Kaim, W.; Lahiri, G. K. *Chem.—Eur. J.* **2006**, *12*, 489−498.
(34) Kobayashi, T.; Nishina, Y.; Shimizu, K. G.; Satô, G. P. *Chem. Lett.* **1988**, 1137−1140.
(35) Naumann, C.; Langhals, H. *Synthesis* **1990**, 279−281.
(36) Sheldrick, G. M. *Acta Crystallogr., Sect. A* **2008**, *A64*, 112−122. (b) *Program for Crystal Structure Solution and Refinement;* University of Goettingen: Goettingen, Germany, 1997.
(37) Lee, C.; Yang, W.; Parr, R. G. *Phys. Rev. B* **1988**, *37*, 785−789.

(38) (a) Andrae, D.; Haeussermann, U.; Dolg, M.; Stoll, H.; Preuss, H. *Theor. Chim. Acta* **1990**, *77*, 123−141. (b) Fuentealba, P.; Preuss, H.; Stoll, H.; Szentpaly, L. V. *Chem. Phys. Lett.* **1989**, *89*, 418−422.
(39) Frisch, M. J.; Trucks, G. W.; Schlegel, H. B.; Scuseria, G. E.; Robb, M. A.; Cheeseman, J. R.; Scalmani, G.; Barone, V.; Mennucci, B.; Petersson, G. A.; Nakatsuji, H.; Caricato, M.; Li, X.; Hratchian, H. P.; Izmaylov, A. F.; Bloino, J.; Zheng, G.; Sonnenberg, J. L.; Hada, M.; Ehara, M.; Toyota, K.; Fukuda, R.; Hasegawa, J.; Ishida, M.; Nakajima, T.; Honda, Y.; Kitao, O.; Nakai, H.; Vreven, T.; Montgomery Jr., J. A.; Peralta, J. E.; Ogliaro, F.; Bearpark, M.; Heyd, J. J.; Brothers, E.; Kudin, K. N.; Staroverov, V. N.; Kobayashi, R.; Normand, J.; Raghavachari, K.; Rendell, A.; Burant, J. C.; Iyengar, S. S.; Tomasi, J.; Cossi, M.; Rega, N.; Millam, J. M.; Klene, M.; Knox, J. E.; Cross, J. B.; Bakken, V.; Adamo, C.; Jaramillo, J.; Gomperts, R.; Stratmann, R. E.; Yazyev, O.; Austin, A. J.; Cammi, R.; Pomelli, C.; Ochterski, J. W.; Martin, R. L.; Morokuma, K.; Zakrzewski, V. G.; Voth, G. A.; Salvador, P.; Dannenberg, J. J.; Dapprich, S.; Daniels, A. D.; Farkas, O.; Foresman, J. B.; Ortiz, J. V.; Cioslowski, J.; Fox, D. J. *Gaussian 09;* (Revision A.02); Gaussian, Inc.: Wallingford, CT, 2009.
(40) (a) Bauernschmitt, R.; Ahlrichs, R. *Chem. Phys. Lett.* **1996**, *256*, 454−464. (b) Stratmann, R. E.; Scuseria, G. E.; Frisch, M. J. *J. Chem. Phys.* **1998**, *109*, 8218−8225. (c) Casida, M. E.; Jamorski, C.; Casida, K. C.; Salahub, D. R. *J. Chem. Phys.* **1998**, *108*, 4439−4450.
(41) (a) Barone, V.; Cossi, M. *J. Phys. Chem. A* **1998**, *102*, 1995−2001. (b) Cossi, M.; Barone, V. *J. Chem. Phys.* **2001**, *115*, 4708−4718. (c) Cossi, M.; Rega, N.; Scalmani, G.; Barone, V. *J. Comput. Chem.* **2003**, *24*, 669−681.
(42) Leonid, S. *Chemissian 1.7;* 2005−2010. http://www.chemissian.com (accessed Sep, 2013).
(43) Zhurko, D. A.; Zhurko, G. A. *ChemCraft 1.5;* Plimus: San Diego, CA. http://www.chemcraftprog.com (accessed Sep, 2013).